Integration of Bridge Damage Detection Concepts and Components

Volume I: Strain-Based Damage Detection

BRIDGE ENGINEERING CENTER

Final Report 1 of 3
October 2013

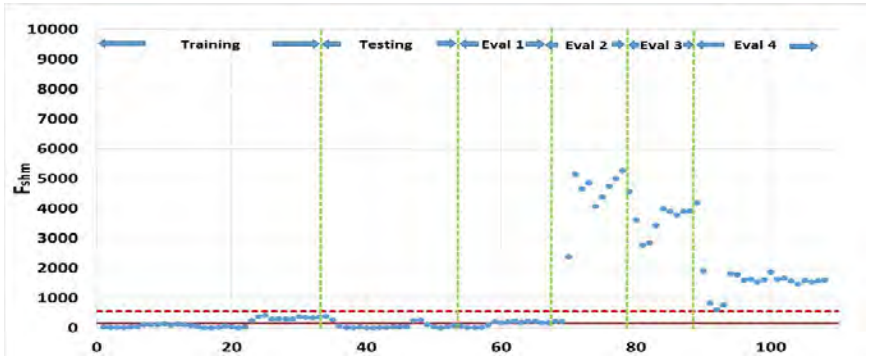

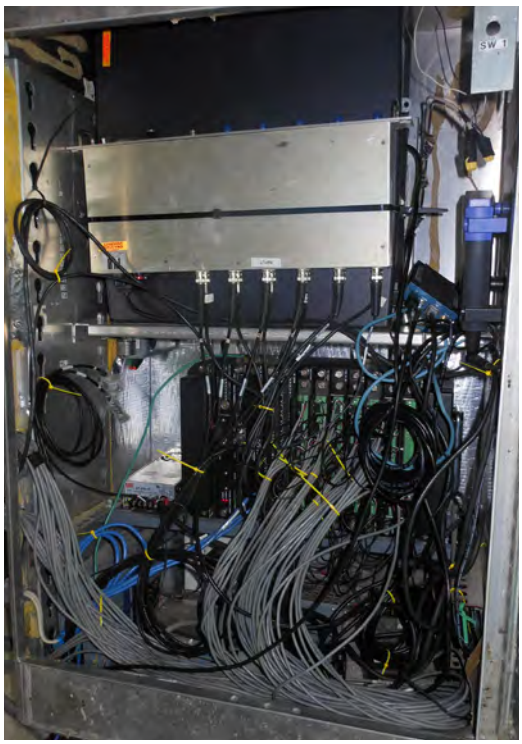

IOWA STATE UNIVERSITY
Institute for Transportation

Sponsored by
Iowa Highway Research Board
(IHRB Project TR-636)
Iowa Department of Transportation
(InTrans Project 11-416)

About the BEC

The mission of the Bridge Engineering Center is to conduct research on bridge technologies to help bridge designers/owners design, build, and maintain long-lasting bridges.

Disclaimer Notice

The contents of this report reflect the views of the authors, who are responsible for the facts and the accuracy of the information presented herein. The opinions, findings and conclusions expressed in this publication are those of the authors and not necessarily those of the sponsors.

The sponsors assume no liability for the contents or use of the information contained in this document. This report does not constitute a standard, specification, or regulation.

The sponsors do not endorse products or manufacturers. Trademarks or manufacturers' names appear in this report only because they are considered essential to the objective of the document.

Non-Discrimination Statement

Iowa State University does not discriminate on the basis of race, color, age, religion, national origin, sexual orientation, gender identity, genetic information, sex, marital status, disability, or status as a U.S. veteran. Inquiries can be directed to the Director of Equal Opportunity and Compliance, 3280 Beardshear Hall, (515) 294-7612.

Iowa Department of Transportation Statements

Federal and state laws prohibit employment and/or public accommodation discrimination on the basis of age, color, creed, disability, gender identity, national origin, pregnancy, race, religion, sex, sexual orientation or veteran's status. If you believe you have been discriminated against, please contact the Iowa Civil Rights Commission at 800-457-4416 or Iowa Department of Transportation's affirmative action officer. If you need accommodations because of a disability to access the Iowa Department of Transportation's services, contact the agency's affirmative action officer at 800-262-0003.

The preparation of this report was financed in part through funds provided by the Iowa Department of Transportation through its "Second Revised Agreement for the Management of Research Conducted by Iowa State University for the Iowa Department of Transportation" and its amendments.

The opinions, findings, and conclusions expressed in this publication are those of the authors and not necessarily those of the Iowa Department of Transportation.

Technical Report Documentation Page

1. Report No.	2. Government Accession No.	3. Recipient's Catalog No.
IHRB Project TR-636		

4. Title and Subtitle	5. Report Date
Integration of Bridge Damage Detection Concepts and Components Volume I: Strain-Based Damage Detection	October 2013
	6. Performing Organization Code

7. Author(s)	8. Performing Organization Report No.
Brent M. Phares, Lowell Greimann, and Hyungjoo Choi	InTrans Project 11-416

9. Performing Organization Name and Address	10. Work Unit No. (TRAIS)
Bridge Engineering Center Iowa State University 2711 South Loop Drive, Suite 4700 Ames, IA 50010-8664	**11. Contract or Grant No.**

12. Sponsoring Organization Name and Address	13. Type of Report and Period Covered
Iowa Highway Research Board Iowa Department of Transportation 800 Lincoln Way Ames, IA 50010	Final Report 1 of 3
	14. Sponsoring Agency Code IHRB Project TR-636

15. Supplementary Notes

Visit www.intrans.iastate.edu for color pdfs of this and other research reports.

16. Abstract

In this work, a previously-developed structural health monitoring (SHM) system was advanced toward a ready-for-implementation system. Improvements were made with respect to automated data reduction/analysis, data acquisition hardware, sensor types, and communication network architecture.

The statistical damage-detection tool, control-chart-based damage-detection methodologies, were further investigated and advanced. For the validation of the damage-detection approaches, strain data were obtained from a sacrificial specimen attached to the previously-utilized US 30 Bridge over the South Skunk River (in Ames, Iowa), which had simulated damage,. To provide for an enhanced ability to detect changes in the behavior of the structural system, various control chart rules were evaluated. False indications and true indications were studied to compare the damage detection ability in regard to each methodology and each control chart rule.

An autonomous software program called Bridge Engineering Center Assessment Software (BECAS) was developed to control all aspects of the damage detection processes. BECAS requires no user intervention after initial configuration and training.

17. Key Words	18. Distribution Statement
assessment software—BECAS—control chart based—damage-detection methodology—false-indication rate—SHM—structural health monitoring—true-indication rate	No restrictions.

19. Security Classification (of this report)	20. Security Classification (of this page)	21. No. of Pages	22. Price
Unclassified.	Unclassified.	79	NA

Form DOT F 1700.7 (8-72) **Reproduction of completed page authorized**

THREE-VOLUME REPORT ABSTRACT

The Iowa Department of Transportation (DOT) started investing in research (through both the Iowa Highway Research Board and the Office of Bridges and Structures) in 2003 to develop a structural health monitoring (SHM) system capable of identifying damage and able to report on the general operational condition of bridges. In some cases, the precipitous for these developments has been a desire to avoid damage that might go unnoticed until the next biennial inspection. Of specific and immediate concern was the state's inventory of fracture-critical structures.

The goal of this project was to bring together various components of recently-completed research at Iowa's Regent Universities with the following specific objectives:

- Final development of the overall SHM system hardware and software
- Integration of vibration-based measurements into current damage-detection algorithm
- Evaluation and development of energy-harvesting techniques

The three-volume final report summarizes the results of this project as follows:

Volume I: Strain-Based Damage Detection, from the Iowa State University Bridge Engineering Center, reviews information important to the strain-based SHM methodologies, details the upgraded damage-detection hardware and software system, demonstrates the application of the control-chart-based methodologies developed, and summarizes the results in graphical and tabular formats.

Volume II: Acceleration-Based Damage Detection, from the University of Iowa Center for Computer-Aided Design, presents the use of vibration-based damage-detection approaches as local methods to quantify damage at critical areas in structures. Acceleration data were collected and analyzed to evaluate the relationships between sensors and with changes in environmental conditions. A sacrificial specimen was investigated to verify the damage-detection capabilities and this volume presents a transmissibility concept and damage-detection algorithm that show potential to sense local changes in the dynamic stiffness between points across a joint of a real structure.

Volume III: Wireless Bridge Monitoring Hardware, from the University of Northern Iowa, Electrical Engineering Technology, summarizes the energy harvesting techniques and prototype development for a bridge monitoring system that uses wireless sensors. The functions and performance of the developed system, including strain data, energy harvesting capacity, and wireless transmission quality, are covered in this volume.

INTEGRATION OF BRIDGE DAMAGE DETECTION CONCEPTS AND COMPONENTS VOLUME I: STRAIN-BASED DAMAGE DETECTION

Final Report 1 of 3
October 2013

Principal Investigator
Brent M. Phares, Director
Bridge Engineering Center, Iowa State University

Co-Principal Investigators
Salam Rahmatalla, Associate Professor
Civil and Environmental Engineering, Center for Computer-Aided Design, University of Iowa

Jin Zhu, Associate Professor
Electrical Engineering Technology, University of Northern Iowa

Ping Lu, Rating Engineer
Office of Bridges and Structures, Iowa Department of Transportation

Research Assistant
Hyungjoo Choi

Authors
Brent M. Phares, Lowell Greimann, and Hyungjoo Choi

Sponsored by
the Iowa Highway Research Board and Iowa Department of Transportation
(IHRB Project TR-636)

Preparation of this report was financed in part
through funds provided by the Iowa Department of Transportation
through its Research Management Agreement with the
Institute for Transportation
(InTrans Project 11-416)

A report from
Institute for Transportation
Iowa State University
2711 South Loop Drive, Suite 4700
Ames, IA 50010-8664
Phone: 515-294-8103 Fax: 515-294-0467
www.intrans.iastate.edu

TABLE OF CONTENTS

LIST OF FIGURES

LIST OF TABLES

ACKNOWLEDGMENTS

The authors would like to thank the Iowa Highway Research Board (IHRB) and Iowa Department of Transportation (DOT) for sponsoring this research. The authors would also like the thank Ahmad Abu-Hawash and many other members of the Iowa DOT Office of Bridges and Structures for their continued support of this research.

EXECUTIVE SUMMARY

An experimental validation for an autonomous damage-detection algorithm, known as the cross prediction methodology, was completed on the US 30 Bridge over the South Skunk River in Ames, Iowa on a previous project. To validate the accuracy of the control-chart-based damage-detection algorithm, sacrificial specimens were fabricated and damaged. To improve the damage detection ability of the methodology with respect to false-indication readings a statistical f-test was introduced.

In this work, a complete structural health monitoring (SHM) system was finalized with hardware and software components. For example, the previously-used fiber-optic sensors were replaced with traditional strain gauge and the external communication system was upgraded to include automated file transfer using fourth generation (4G) cellular technology.

A complete software package named Bridge Engineering Center Assessment Software (BECAS) was developed and includes multiple automated damage-detection processes including sensor data acquisition, strain range data reduction, and statistical control-chart-based evaluation, based on damage-detection methodologies. The damage detection ability was updated to include multiple, redundant methods including: 1) one-truck event, 2) truck events grouped by ten, 3) cross prediction, and 4) F_{shm} method. Each of these methods were investigated and then analyzed in terms of false-indication rate and control chart rules.

As possibly the most intuitive damage-detection method, the one-truck event methodology involves the construction of control charts using the strain range data for individual truck events. For the truck events grouped by ten method, control charts are created in a similar way, but by averaging 10 successive truck passages to create a single data point. Both the one-truck event method and the truck events grouped by ten method had relatively low false-indication rates and were able to detect damage. In the cross prediction and F_{shm} methods, the major improvement was made in the use of orthogonal regression instead of traditional linear regression. Both methods showed a comparatively higher number of false indications than the previous two methods but also had significant increases in the number of true indications.

The cross prediction and F_{shm} methods had a relatively large number of false indications at sensors in the cut-back web-gap region of the bridge. To have a better understanding of the cause of the false indication, the cut-back web-gap region was inspected using visual and magnetic particle techniques. A small crack-like indication near the cut-back web-gap region was identified and might be actual damage detected by the system. Further study of the false-indication rate was conducted by removing the cut-back region data.

1. INTRODUCTION

1.1 General Background

Bridge structural health monitoring (SHM), which typically includes specialized hardware and software algorithms, has been widely investigated during the past two decades. Many SHM techniques have been proposed as a means to provide methods to increase the overall safety of bridges. These developments have been driven, in part, by a desire to have continuous feedback on system performance that provides for a more reliable and robust transportation system. In addition, it has been shown that periodic visual inspections may not be as reliable as desired (Lu 2008).

Since 2003, strain-based damage-detection algorithms for the US 30 Bridge over the South Skunk River in Ames, Iowa have been studied and developed by the Iowa State University Bridge Engineering Center. For the first generation of the damage-detection algorithm, a long-term monitoring system was developed that included novel data management processes including automated data zeroing, filtering, and extrema identification (Doornink 2006).

To improve the detection capabilities and to remove user subjectivity, two important advancements were made in a second-generation system. First, a powerful vehicle-identification system was developed and, second, the algorithm was quantified statistically. The statistical-based damage-detection methodology, named the cross prediction method (using control chart) was formulated by Lu (2008).

In 2010, an experimental validation was conducted to study the efficacy of the approaches. Sacrificial specimens were mounted to an in-service bridge and exposed to real traffic loads with fatigue cracks and thickness loss damage induced (Phares et. al 2011). The results showed that the damage-detection algorithm detects structural damage well. Unfortunately, a relatively high false-indication rate was also observed. Therefore, improvements to the algorithm were investigated and evaluated. The statistical f-test was proposed as a means to improve overall system performance (Phares et. al 2011).

In the work summarized herein, the damage-detection process based on statistical control charts, using continuous strain range data, was further developed. False-indication and true-indication rates were more fully investigated and then compared. The previous SHM sensor system (fiber-optic sensors) was replaced with new hardware systems (conventional resistance sensors) for operational verification. In addition, turnkey software was developed to control the entire damage-detection process autonomously.

1.2 Objective of Research

The objective of this research was to finalize the development of the overall SHM system on the US 30 Bridge including the hardware, software, and damage-detection methodology. New hardware (including sensor, data acquisition, and communication architecture) was configured,

installed, and verified operationally on an in-service bridge. Four strain-based damage-detection methodologies, one-truck event, truck events grouped by ten, cross prediction, and f-test, were investigated and compared using control chart theory. A complete software package called Bridge Engineering Center Assessment Software (BECAS) was developed to form an integrated SHM system.

1.3 Organization of Report

In this report, Chapter 2 reviews information important to the strain-based SHM methodologies and Chapter 3 details the upgraded damage-detection hardware and software system. Chapter 4 demonstrates the application of the control-chart-based methodologies developed and summarizes the results in graphical and tabular formats. Chapter 5 summarizes this project and presents conclusions and recommendations based on all aspects of the work.

2. PERTINENT LITERATURE REVIEW

This chapter, which serves as a review of relevant work to date, is divided into three primary subsections. The first describes what is known as the cross prediction model control chart methodology for detecting damage. The second summarizes previous work completed to validate the damage detection approaches. The third presents information related to the use of orthogonal regression and how that has been used in the evolution of the damage-detection approach discussed herein.

2.1 Cross Prediction Model Control Chart Method

2.1.1 Strain Data Identification

In 2007, an SHM system for detecting damage autonomously was developed by Wipf, Phares, and Doornink that used strain as the monitoring metric (Wipf et al. 2007). The bridge used during this development is the eastbound US 30 Bridge crossing the South Skunk River in Ames, Iowa. The US 30 Bridge has three spans with two equal outer spans (97.5 ft each) and a longer middle span (125 ft), a width of 30 ft, and a right-ahead skew of 20 degrees. Figure 2.1 shows a basic plan view of the US 30 Bridge.

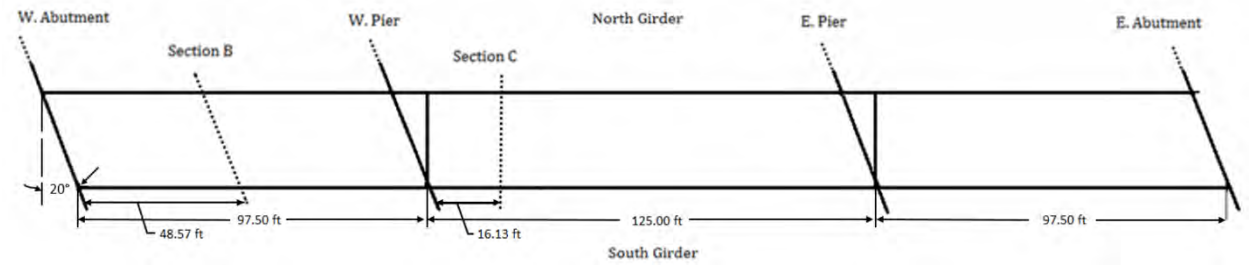

Figure 2.1. Basic plan view of the US 30 Bridge

A total of 40 fiber-optic strain gauges were installed on the bridge in 2007. A unique naming convention for each sensor indicates its location. For example, B-NG-BF-H represents the sensor located at Section B (B-), North girder (NG-), bottom flange (BF-), horizontal orientation (H). Full details for the sensor locations and orientations are shown in Appendix A. The complete monitoring system is described more fully by Doornink (2006), Lu (2008), and Phares et al. (2011).

The data collection process developed includes a novel approach for data zeroing, filtering, and extrema identification. Data zeroing is performed to remove temperature effects and was accomplished by subtracting a constant temperature offset from data collected in small increments. Then, data filtering is conducted to obtain a data set that represents the quasi-static response of the bridge under ambient traffic loads. The strain data from each vehicular event are then decimated to just the maximum and minimum strain values.

To develop relationships between two sensors, target sensor (TSs), where damage might be expected, and non-target sensors (NTSs) are designated. The "training" process defines the "normal" behavior of the system with relationship limits for each sensor pair determined manually by an engineer. Examples of matched data from two sensors with limits are shown in Figure 2.2.

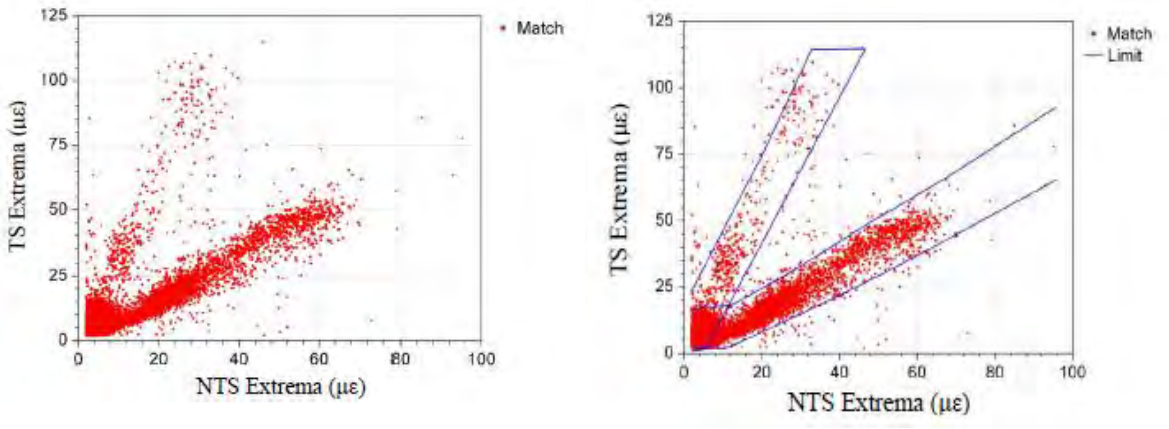

Figure 2.2. Example of matched data from two sensors with applied limits (right) (Wipf et al. 2007)

Following training, during which the limits of normal behavior are defined, subsequent truck events are then compared to the limits. A Pass assessment defines a point within the limits and a Fail assessment defines data outside of the limits. For analytical verification of this general approach, Vis (2007) developed a finite element (FE) model with simulated damage in *Evaluation of a Structural Health Monitoring System for Steel Girder Bridges*. His work showed that some natural variability existed due to truck parameters such as the number of axles and the transverse position of the truck (e.g., left lane or right lane). It was indicated that removing this variability would likely enhance damage-detection ability.

2.1.2 Truck Parameter Identification

To address uncertainties identified by Vis, a second-generation damage-detection algorithm was investigated/developed by Lu (2008) that sought to improve the approach by identifying important truck parameters, which would then be used to reduce the uncertainties. Truck parameters of interest were defined as the travel lane, number of axles, speed, axle spacing, and truck weight. The truck travel lane was determined from the sensor on the girder closest to the vehicle travel lane because it consistently produced a high peak strain and the best truck axle detection algorithm utilized sensors placed on the bottom of the deck near the truck wheel line.

Truck weight could only be estimated as either heavy or light due to the difficulty in assessing the specific weight of each axle accurately. With the truck information determined, the algorithm developed by Lu utilized strain data resulting from only right-lane, five-axle heavy trucks. Lu (2008) also determined that strain range (i.e., the difference between the maximum and minimum

strain during the truck event) is a more effective means of detecting damage than using both the maximum and minimum strains.

2.1.3 Control Charts

With the strain ranges from sensor pairs, a linear prediction model was developed to predict the relationship between two sensor strain range pairs for multiple trucks. The residual was then defined as the difference between the measured strain range and the predicted strain range data as shown in Equation 2-1.

$$Residual(i,j) = Measured\ strain\ range(i,j) - Predicted\ strain\ range(i,j) \quad \textbf{(2-1)}$$

An n × n residual matrix could then be created for each truck event. The information was reduced to an n degree vector, in which element i represented the residual for sensor i and was defined to be the combined-sum residual equal to the sum of row i minus the sum of column i for each truck. Sample distributions of the combined-sum-residuals are shown in Figure 2.3.

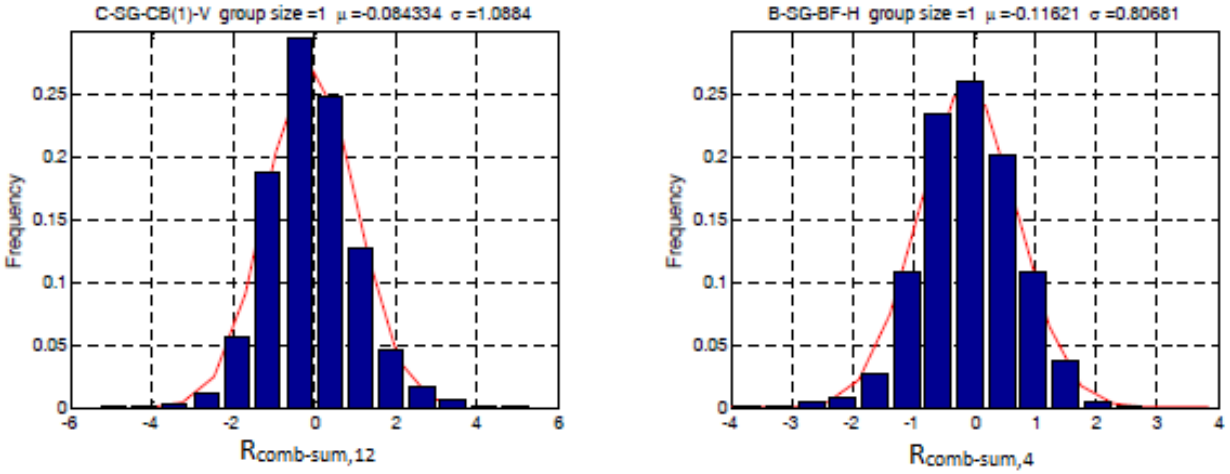

a. Sensor S-SG-CB(1)-V b. Sensor B-SG-BF-H

Figure 2.3. Sample distribution of the combined-sum-residuals (Lu 2008)

With the n-degree vectors, one for each truck, consisting of the combined-sum residual, Shewhart $\overline{x}$ control charts, typically used for process control, could be constructed as a strategically-defined damage indicator for each sensor by plotting the residual values versus truck event. As is common practice, multiple events were usually grouped together to form one point on these charts. In this work, a group size of 10 consecutive trucks for each point was used. Based on the observed normal distribution pattern in Figure 2.3, the upper control limit (UCL) and lower control limit (LCL) were set as shown in Equation 2-2.

$$\begin{cases} UCL = \overline{R} + 3s \\ LCL = \overline{R} - 3s \end{cases} \quad \textbf{(2-2)}$$

where $\overline{R}$ and s is the mean and standard deviation of the combined-sum residuals, respectively. A sample control chart is shown in Figure 2.4.

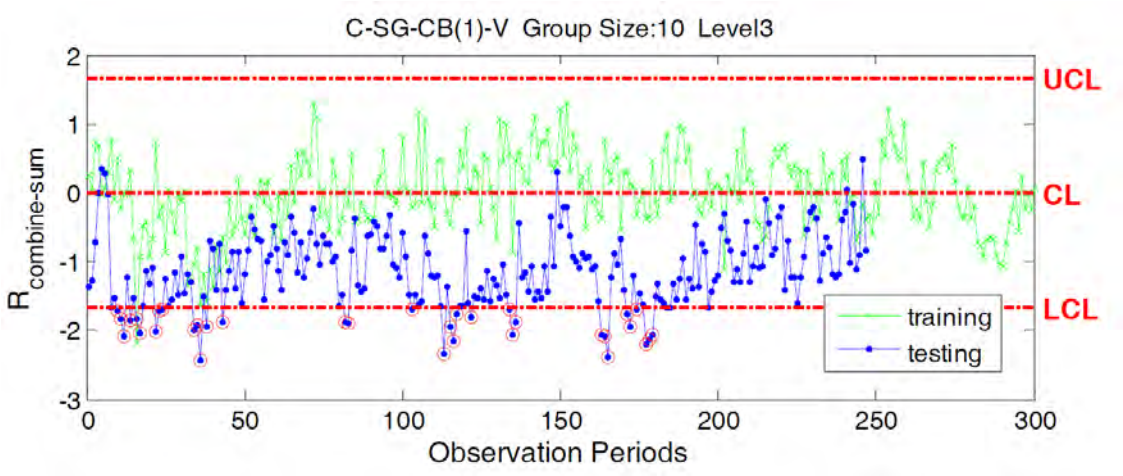

Figure 2.4. Sample control chart (Lu 2008)

Out of limit points on the constructed control charts were defined as an indication of possible structural damage. The probability of detection (POD), which is the ratio of number of detections to the total number of events, was used as a check of the sensitivity of the damage-detection method.

2.2 Methodology Validation

To validate the damage-detection algorithm with actual damage data, two sacrificial specimens, simulating the floor-beam web-gap region in the US 30 Bridge, were fabricated (Phares et al. 2011). Each was integrated into the bridge in such a way that it responded to traffic loads but did not create a safety concern with the introduction of damage. The sacrificial specimen consists of two web-gaps connected by a steel plate. In this configuration, the sacrificial specimen simulates the double curvature bending occurring within the web-gap regions. A typical installed sacrificial specimen and double curvature bending phenomena is shown in Figure 2.5.

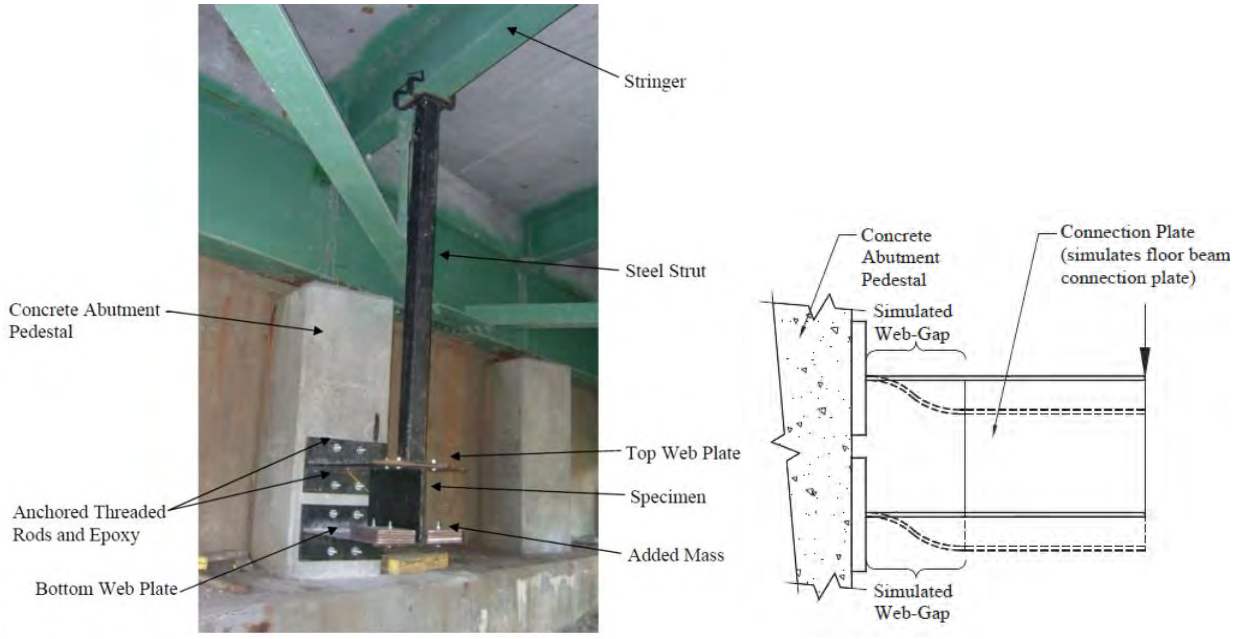

Figure 2.5. Typical installed sacrificial specimen and double curvature bending of sacrificial specimen (Phares et al. 2011)

2.2.1 Sacrificial Specimen 1

Specimen 1 was fabricated with a small electrical discharge machining (EDM) notch through the thickness of the top plate where a crack was expected when high strains and a large number of cycles occurred. It was found that the truck live loading strains in the specimen (and the corresponding real web gap) were insufficient to grow a crack in a reasonable time. Therefore, Specimen 1 was artificially damaged by attaching a rotary shaker to the specimen and cycling the specimen rapidly near its resonance frequency in the range of 60 Hz to 70 Hz. Figure 2.6 and 2.7 show cracking in the top (left) and bottom (right) plates of the sacrificial specimen and information on the installed sensor array, respectively.

Figure 2.6. Sacrificial Specimen 1 cracking (Phares et al. 2011)

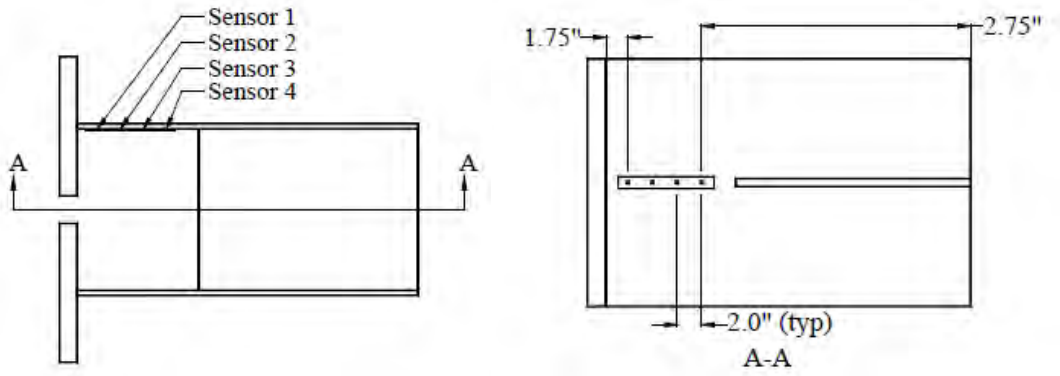

Figure 2.7. Details for sacrificial specimen with sensor array (Phares et al. 2011)

2.2.2 Sacrificial Specimen 2

Specimen 2 was constructed identically to Specimen 1, except without an EDM notch. Specimen 2 was vibrated to create different levels of damage occurring in the web-gap area: no crack, 1.25 in. crack, 1.50 in. crack, and 1.75 in. crack. After each crack increment, data for heavy, right-lane, five-axle trucks were collected for several days. A photograph of the sacrificial Specimen 2 top web plate cracking is shown in Figure 2.8.

Figure 2.8. Sacrificial Specimen 2 top web plate cracking (Phares et al. 2011)

The cross prediction methodology described in Section 2.1 was applied to the data from both Specimen 1 and 2 to evaluate its effectiveness in detecting damage. The methodology worked quite well but results revealed relatively high false-indication rates (Phares et al. 2011). As a result, the authors suggested improvements to the methodology, as summarized below.

2.3 Orthogonal Regression and Statistical Evaluation Approach

Using orthogonal linear regression and the statistical f-test were proposed and developed to reduce the relatively high false-detection rate associated with the previously-described cross prediction damage-detection method. It was believed that these two methods would further reduce uncertainties in the cross prediction methodology and, therefore, reduce the false-positive rate.

2.3.1 Development of Orthogonal Regression and Orthogonal Residual

The most common use of orthogonal linear regression is in comparing two measurement systems that both have measurement variations (Carroll and Ruppert 1996). In other words, the y measurement variation and the x measurement variation are both the same. A standard linear regression assumes that the x variable is fixed (i.e., no variation) and the y variable is a function of x plus variation. Figure 2.9 shows samples of standard linear regression and orthogonal linear regression.

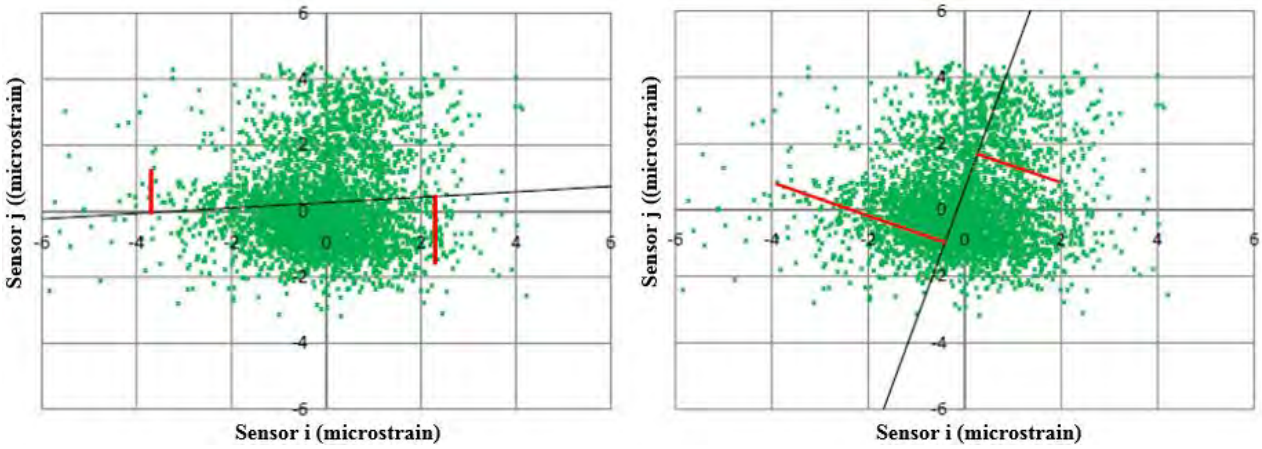

Figure 2.9. Sample standard linear regression (left) and sample orthogonal linear regression (right) (Phares et al. 2011)

The vertical bars in the chart on the left represent the y-residual and the negatively-sloping line in the chart on the right represents the orthogonal residual. As with any linear regression, y and x are related linearly through the following equation:

$$y = b + mx \qquad \textbf{(2-3)}$$

where b is the y-intercept and m is the slope.

The equation for standard linear regression can be developed by minimizing the sum of the square of the y-residual, while the sum of the square of the perpendicular residual is minimized in the orthogonal linear regression.

$$r_i = \frac{y_i - b - mx_1}{\sqrt{m^2+1}} \quad \textbf{(2-4)}$$

When the strain range data are in the first quadrant, an orthogonal residual is defined. An example of an orthogonal line fit and an orthogonal residual is shown in Figure 2.10.

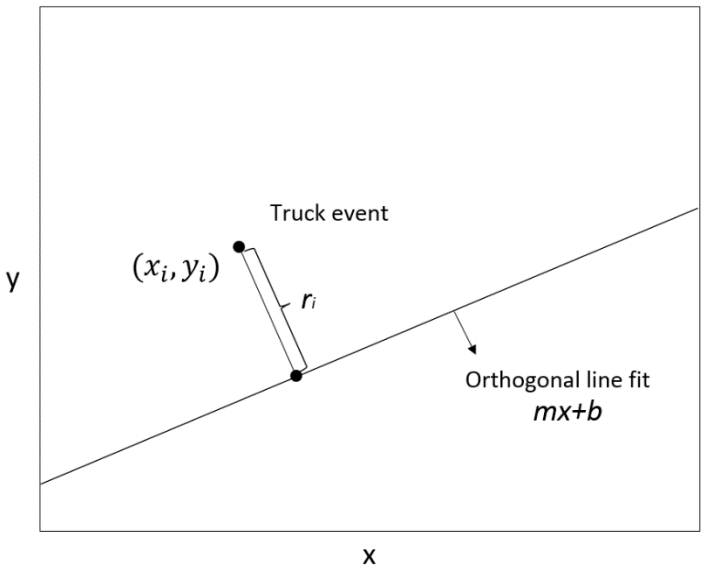

Figure 2.10. Example of an orthogonal line fit and an orthogonal residual

The sum of square of the perpendicular residuals r_i (SSR) from the data points to the regression line are given by the following:

$$SSR = \sum_{i=1}^{n} {r_i}^2 \quad \textbf{(2-5)}$$

Minimizing SSR results in the following (Carroll and Ruppert 1996 and Fuller 1987):

$$m = \frac{{s_x}^2 - {s_y}^2 + \{({s_x}^2 - {s_y}^2)^2 + 4{s_{xy}}^2\}^{\frac{1}{2}}}{2s_{xy}} \quad \textbf{(2-6)}$$

$$b = \overline{y} - m\overline{x} \quad \textbf{(2-7)}$$

where ${s_x}^2$ and ${s_y}^2$ are the variance of the x and y data, respectively and s_{xy} is the covariance of x and y that can be written $\rho_{xy} s_x s_y$ in which ρ_{xy} is the correlation coefficient.

2.3.2 Damage Detection Approach with f-test

The f-test is typically used to evaluate the relationship between two different data sets (Mendenhall and Sincich 2012). Generally, the purpose of the f-test is to quantify the amount of model improvement achieved by including additional variables in the prediction model by

comparing the sum of the square of the residual (SSR) of a reduced and a full model with respect to each one's degree(s) of freedom. The full model (the more complex one), which contains more variables than the reduced model (the simpler one) was developed with a Z factor, which is an indicator variable and taken in (Phares et al. 2011) to be as follows:

$$y = (\alpha_1 + \alpha_3 x) + Z(\alpha_2 + \alpha_4 x) \quad \textbf{(2-8)}$$

when Z is equal to zero, α_1 and α_3 are parameters from an orthogonal linear regression through the training data and, similarly, when Z is equal to one, α_1 plus α_2 and α_3 plus α_4 are the parameters from orthogonal linear regression through the post-training date. Z in this case indicates whether the data were from a training period or following the training period. One requirement for using the f-test is that the reduced model must be nested within the full model. Here the reduced model is taken as follows:

$$y = \alpha_5 + \alpha_6 x \quad \textbf{(2-9)}$$

where $\alpha_5$and α_6 are parameters from an orthogonal linear regression through all the data (training and post training). An example of orthogonal fit lines for the full and reduced models are shown in Figure 2.11.

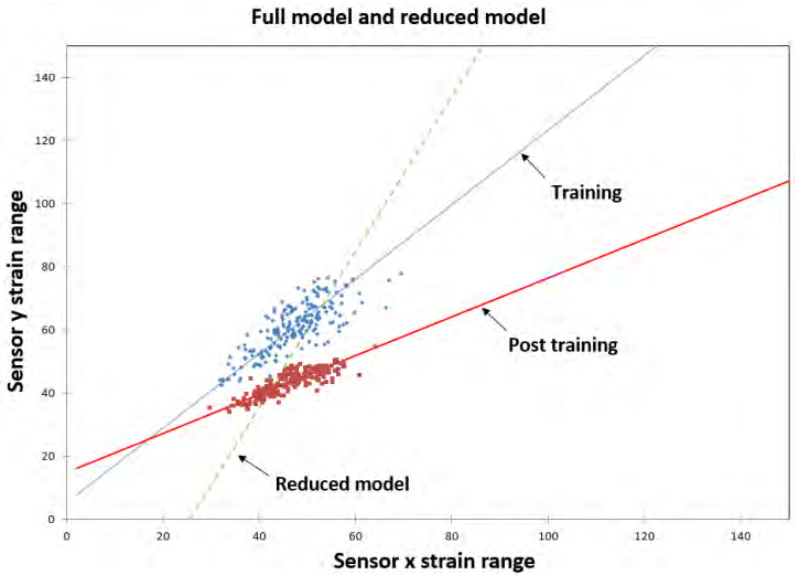

Figure 2.11. Orthogonal fit lines for the full and reduced models

With the given full and reduced model, the similarity hypothesis must be tested:

H_0 (Null hypothesis): $\alpha_2 = \alpha_4 = 0$
H_A (Alternative hypothesis): α_2 *or* $\alpha_4 \neq 0$

If H_0 is true, the reduced model is statistically the same as the full model as shown graphically in Figure 2.12 (left) and it can be concluded that there is no damage at those two sensor locations. On the other hand, if H_0 is rejected, which is graphically illustrated in Figure 2.12, the reduced model is significantly different from the full model and it may be an indication of damage.

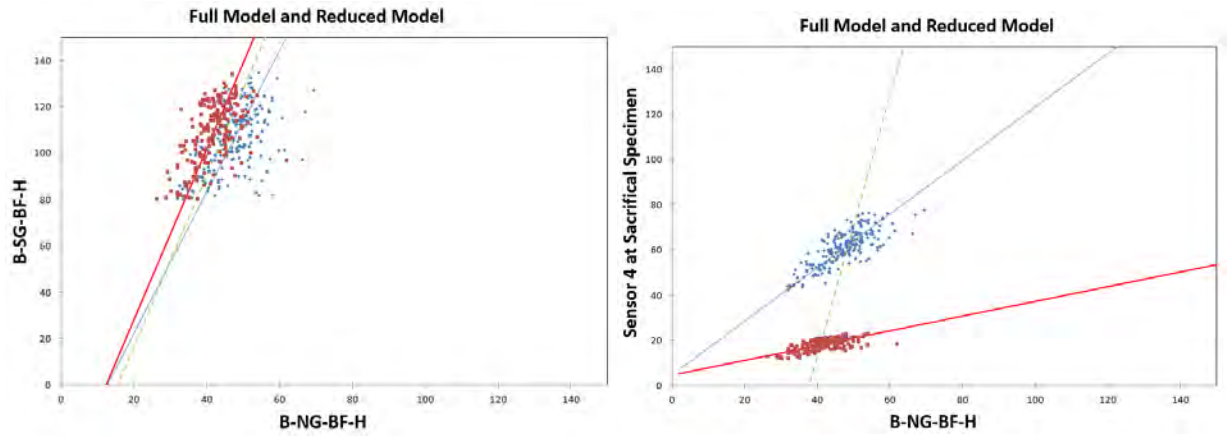

Figure 2.12. Graphical representation of rejecting H_0, no damage (left) and failing to reject H_0, damage (right)

To quantify these results, the f-test is conducted with the null hypothesis ($\alpha_2 = \alpha_4 = 0$) showing that the reduced model is able to fit the data set statistically as well as the full model. In general, the F statistic is defined as follows (Caragea 2007):

$$F = \frac{SSRreduced - SSRfull}{dfreduced - dffull} \div \frac{SSR\,full}{dffull} \quad \textbf{(2-10)}$$

where $SSR_{reduced}$ is the sum of the square of the residual of the reduced model and SSR_{full} is the sum of the square of the residual of the full model as given in Equation 2-5. df is the degrees of freedom associated with an SSR; $df_{reduced}$ and df_{full} are the degrees of freedom of the reduced and full models, respectively. For the case of the models in Equation 2-11:

$$df_{reduced} = n - 2$$

$$df_{full} = n - 4 \quad \textbf{(2-11)}$$

because the reduced model has two terms and the full model has four terms and n represents the number of truck events, that is as follows. Note that SSR_{full} is the sum of the squares of the residuals for both training and post-training data.

$$n = ntraining + npost\ training \quad \textbf{(2-12)}$$
$$ntraining = number\ of\ trucks\ in\ the\ training\ data \quad \textbf{(2-13)}$$
$$npost\ training = number\ of\ trucks\ in\ the\ post\ training\ data \quad \textbf{(2-14)}$$

3. DAMAGE DETECTION HARDWARE AND SOFTWARE

The fiber-optic sensing (FOS) SHM sensor system placed on the US 30 Bridge in 2006 and briefly described in Chapter 2 was removed and replaced with updated hardware and software in 2012 as part of this project. The change in hardware from FOS to more traditional sensors was determined to be a more cost-effective and robust approach. All software developed as part of this project was developed specifically to interface with this hardware system. This chapter presents the system configuration including the SHM hardware and network configuration, and it also illustrates what a typical installation might consist of (using the US 30 Bridge as the case study).

3.1 Hardware

3.1.1 Configuration

The SHM hardware at the US 30 Bridge installed for this work consists of electrical resistance strain gauges that were run through completion bridge modules 4WF120 or 4WF350 depending on the gauge resistance and hard-wired to a Campbell Scientific CR9000x data logger. The data logger used the CR9052 module and programming was completed by using CRBasic language from Campbell Scientific. The CR9052 cards were used specifically because they have the on-board filtering needed when running high-speed acquisitions. This filtering helps in eliminating electrical noise from the signal.

Other hardware components included a typical desktop computer, network switch, router, Sierra Wireless 4G cellular modem, Comtelco dual band panel antenna, and Wilson Yagi antenna. The data logger, network switch, desktop computer, router, and cellular modem were located in an environmentally-controlled cabinet at the bridge. The sensor network of electrical resistance strain gauges and other components are illustrated in Figure 3.1.

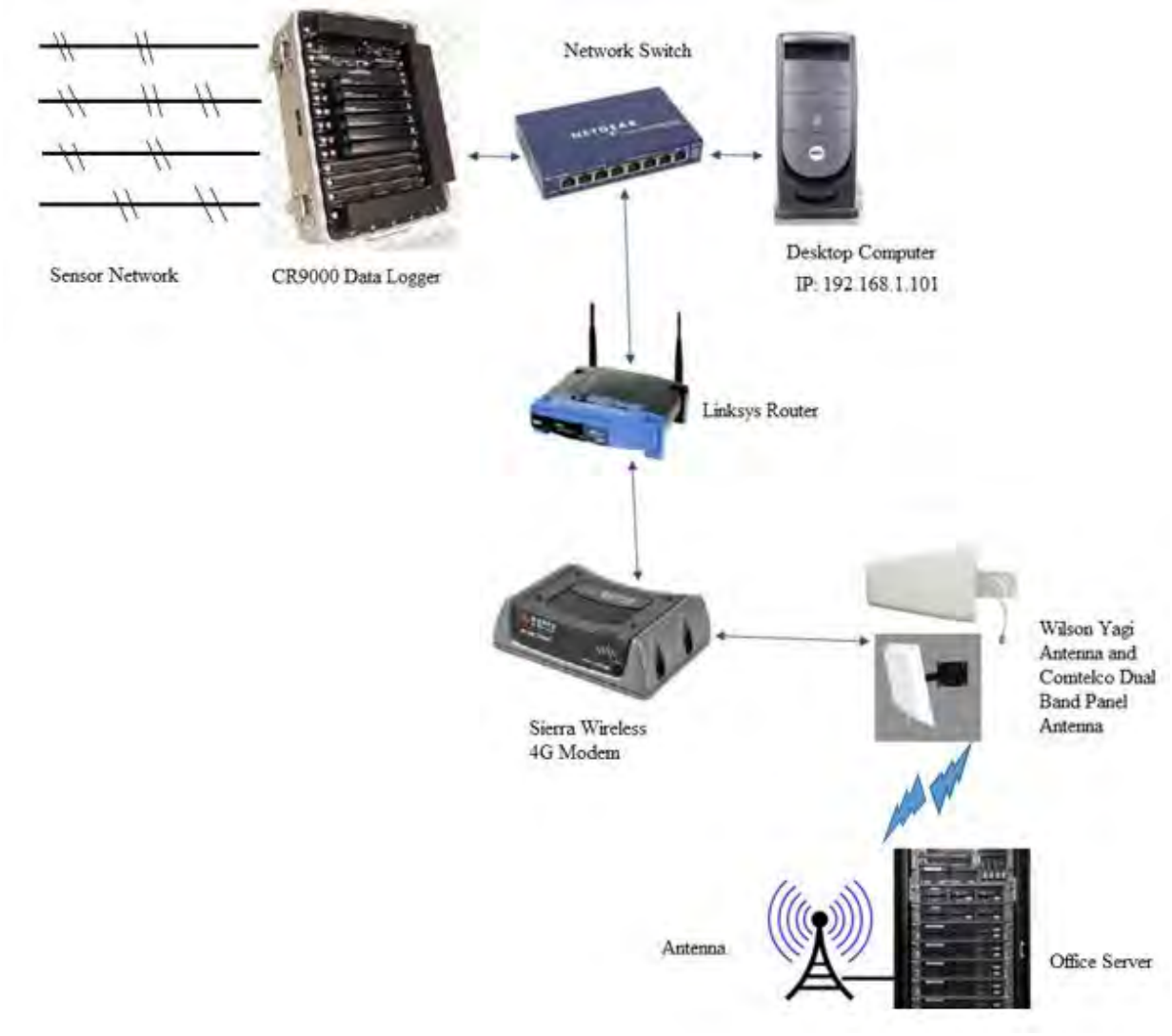

Figure 3.1. SHM system components and system architecture

The data collected by the sensors were transferred from the data logger to the desktop computer via a network switch. Once the data were stored temporarily on the desktop computer, they were sent to the router, via the network switch, and finally to the cellular modem, where they were transmitted to the office server via 4G cellular communication. Note that the purpose of the switch is to connect the data logger directly to the computer without having to go through a router that is also connected to a cellular modem. By connecting the data logger directly to the computer, communication failures can be virtually eliminated.

Data files were formatted as DAT files and collected every minute at a sampling rate of 250 Hz. Relatively new 4G cellular technology enabled files to be transferred in real time (i.e., as quick as the collection rate of every minute). The software controlling the data transfer involves a standard File Transfer Protocol (FTP) with the configuration details given in Appendix B.

3.1.2 Typical Installation

The first step in designing an SHM installation is to identify the goals associated with the installation. Once the goals are identified, particular features of the bridge that are important for achieving the goals can be identified. Finally, an instrumentation plan can be created to capture data from these features.

The instrumentation plan for the US 30 Bridge deployed in this work consisted of 38 electrical resistance strain gauges (120 and 350 ohm) and three thermocouples. An isometric view of the US 30 Bridge and the cross sections of interest are shown in Figures 3.2 and 3.3, respectively.

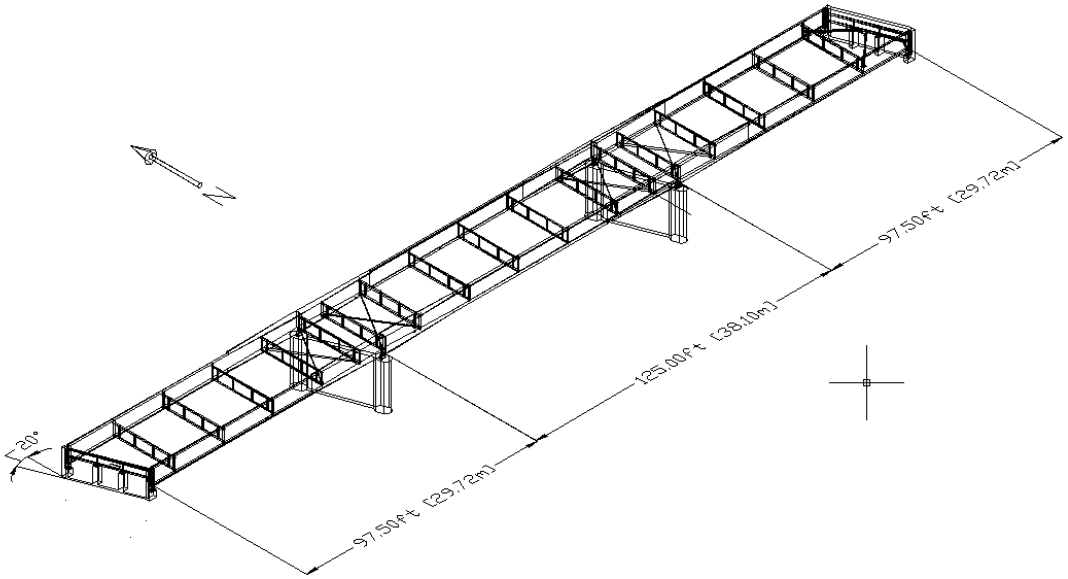

Figure 3.2. Isometric view of US 30 Bridge

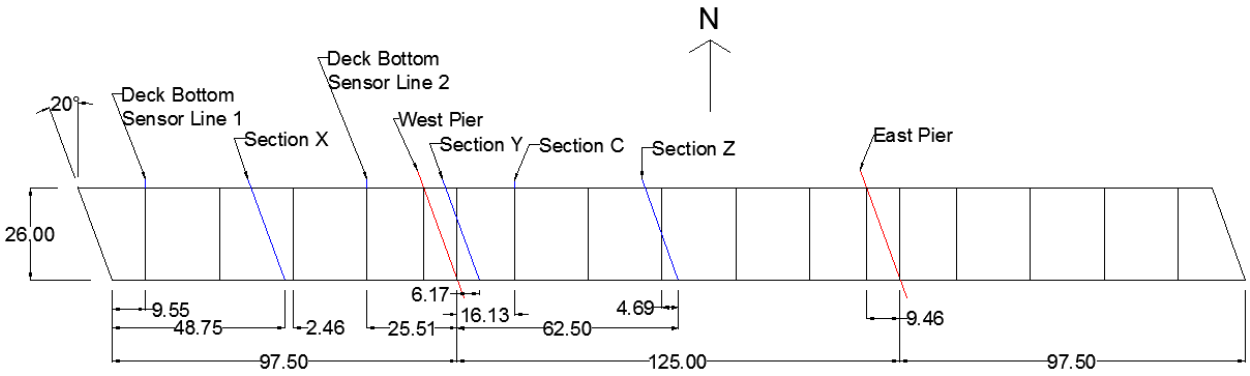

Figure 3.3. Bridge plan view for sensor layout

The strain gauge locations at each of the cross sections are shown in Figure 3.4.

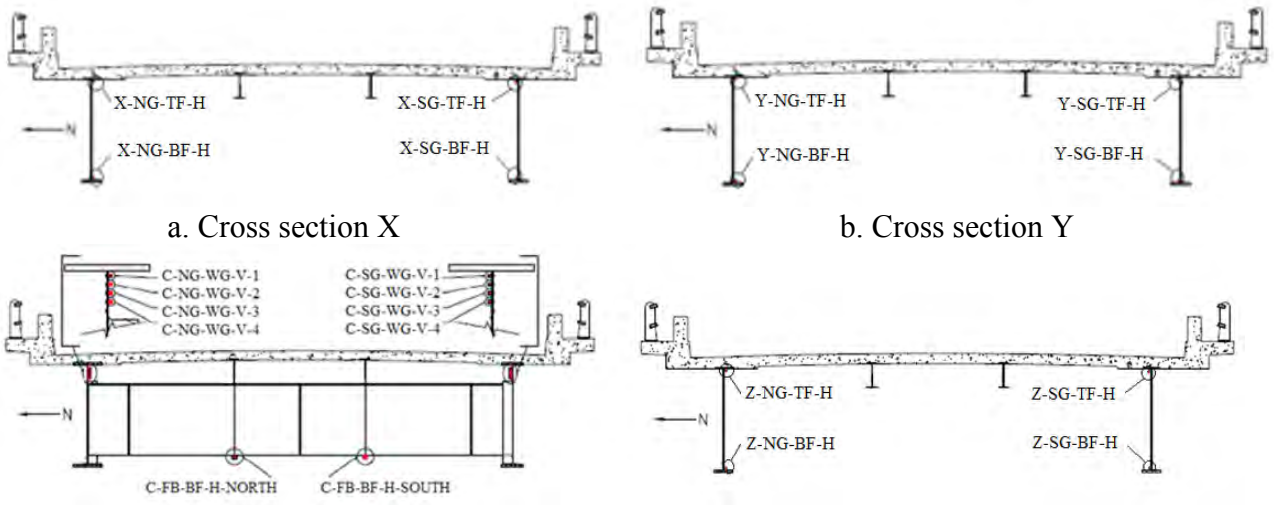

a. Cross section X

b. Cross section Y

c. Cross section C

d. Cross section Z

Figure 3.4. Sensors locations within the bridge framing system

Sections X and Z are at mid-spans given that the maximum bending strains occur near these locations. Section Y was chosen to be close to pier to quantify negative bending effects and continuity behavior. Section C was chosen to capture the web-gap strains, which are of interest because of the behavior in the web-gap cut-back region. Note that Section C is the same as Section C in the FOS instrumentation system described previously. In addition, sensors were placed strategically on the bottom of the deck as illustrated conceptually in Figure 3.5.

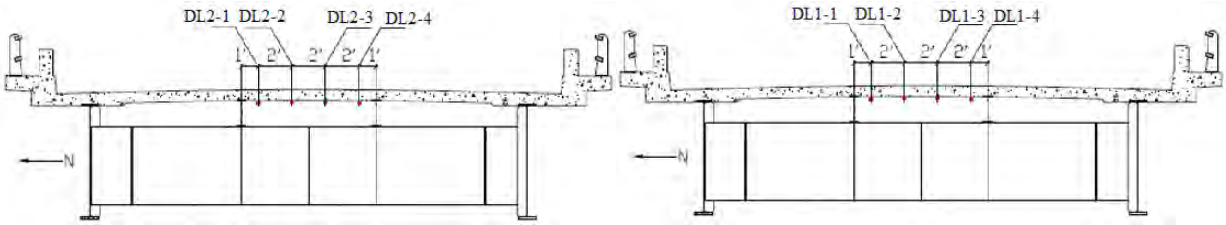

a. Deck bottom sensor line 1

b. Deck bottom sensor line 2

Figure 3.5. Sensor located on the bridge deck bottom

The specific locations of the deck sensors were chosen to identify vehicle travel lane, axle number and spacing, and vehicle speed. Figure 3.6 shows a typical deck bottom sensor and a girder top flange sensor.

Figure 3.6. Deck bottom sensors (left) and sensor installation sample on top flange of girder (right)

For reference, the sensor naming convention was inherited from the FOS naming convention (Chapter 2) and is just one method of naming sensors. In general, any sensor naming system should indicate longitudinal position, transverse position, vertical position, and gauge orientation. The sensor designation used here classfies them into the format: Section-Member-Part-Orientation. For example, B-NG-BF-H represents a sensor installed at section B, north girder (NG), bottom flange (BF), with horizontal (H) orientation. The designation C-NG-WG-V identifies a vertical (V) gauge in the web gap (WG) of the north girder (NG) at cross section C. The thermocouples were placed at section X to measure the air, concrete (mid-depth of deck), and steel temperatures.

3.2 Software

For this project, the development of software that automated the damage-detection process was another main goal. To achieve this, all aspects of the algorithm described here and in other referenced publications were programmed into the BECAS using Microsoft Visual Studio 2010. The software developed includes components that collect, filter, and zero the collected data. Subsequently, individual truck passages are identified using the previously-mentioned truck-detection algorithm. Then, the truck-event data are decimated to strain range values, which then proceed into the various damage-detection algorithms described in the subsequent chapter.

4. DAMAGE-DETECTION METHODOLOGIES

In this chapter, various enhancements to the previously-investigated damage-detection methodologies using control charts are presented and investigated with actual data. The ability of the methodologies to detect damage and the rate at which damage is identified falsely are discussed.

4.1 Overall Methodology

As introduced in Section 2.1, the strain data reduction, which includes data zeroing for removing temperature effects and filtering to obtain the quasi-static response of the bridge, were studied extensively and validated. As part of the overall process, truck parameters were also determined such that only selected five-axle, right-lane trucks are used in the damage-detection approach. In addition, the time-domain data are converted to strain ranges for each truck event. With the strain range data, four control-chart-based damage-detection methods are implemented as shown in the flow chart in Figure 4.1: 1) strain range for a single truck event, 2) strain range for grouped truck events, 3) cross prediction model, and 4) f-test. Details for each of the damage-detection processes are presented in this chapter.

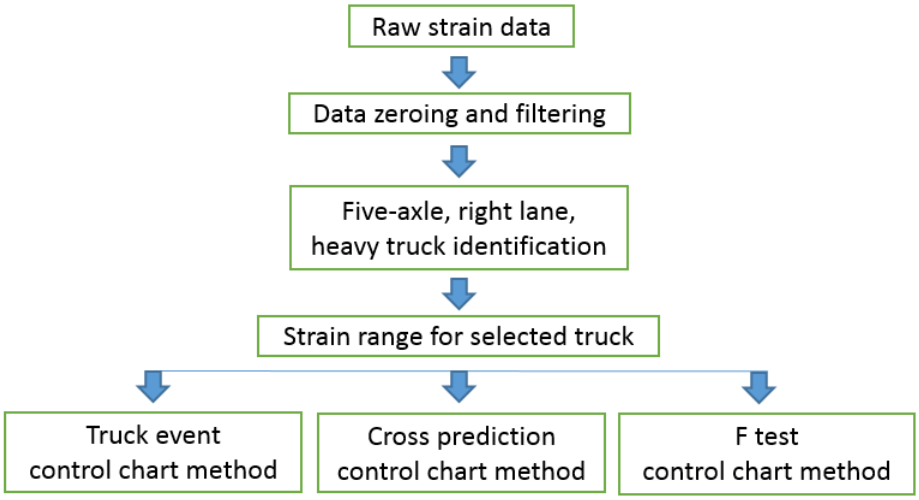

Figure 4.1. Damage-detection methodology

Generally, control charts are used for dealing with measurements and exercising control over the average quality of a process as well as its variability (Miller and Freund 1977). For the damage-detection approach developed here, control charts are divided into three regions: training, testing and evaluation.

The training period, where strain range data are obtained from truck events from the presumed undamaged structure, is used to establish important parameters such as the mean and standard deviation of the measurements, as discussed in Section 2.1.3, to define the normal operation of the system.

Following the training period, a testing period is utilized to evaluate the efficacy of the training period.

The evaluation period is for monitoring the bridge for change in structural performance (e.g., possible damage). In this chapter, evaluation data are further subdivided into the following regions: Evaluation 1, Evaluation 2, Evaluation 3, and Evaluation 4.

For reference, the training period consisted of 2,000 truck events and the testing period consisted of 1,000 truck events. The four evaluation periods represented times when there were varying levels of damage present in the sacrificial Specimen 2. During Evaluation 1, no damage was present. During Evaluation 2, a crack size of 1.25 in. was present. During Evaluation 3, a crack size of 1.50 in. was present. During Evaluation 4, a crack size of 1.75 in. was present. When implemented, the system will operate continuously during the evaluation period with notifications of suspected damage sent in near real-time.

In the previous generation of the control-chart-based damage-detection methodologies, only a single check was used to define when a change in structural behavior had occurred (when data were greater than three standard deviations from the mean). Further investigation into process control led to the realization that some process changes may be missed by only this single rule. (Montogomery 1996) Therefore, additional rules were investigated, formulated, and evaluated. Table 4.1 summarizes the six rules considered during methodology finalization and evaluation.

Table 4.1. Control chart rules (Montogomery 1996) and number of rule checks

Control chart rules	Number of rule checks
#1 – One point beyond ±3s	n
#2 – Two successive points out of three points beyond ±2s	n-3
#3 – Four successive points out of five points ±1s	n-5
#4 – Eight consecutive points on one side of the mean	n-8
#5 – Six consecutive points trending up or down	n-6
#6 – Fourteen consecutive points alternating up or down	n-14

Each of these rules represents a different type of change in process control. In the context of damage detection, the violation of any rule could be an indicator of a change in structural condition.

From the perspective of a structural engineer, a false indication of damage occurs if one of the control chart rules is violated but there is no damage (the incorrect rejection of a true null hypothesis and sometimes called a type I error). For example, the circled points in Figure 4.2 are false indications; that is, they are points outside the control limits but, for this particular case, there is no known structural damage.

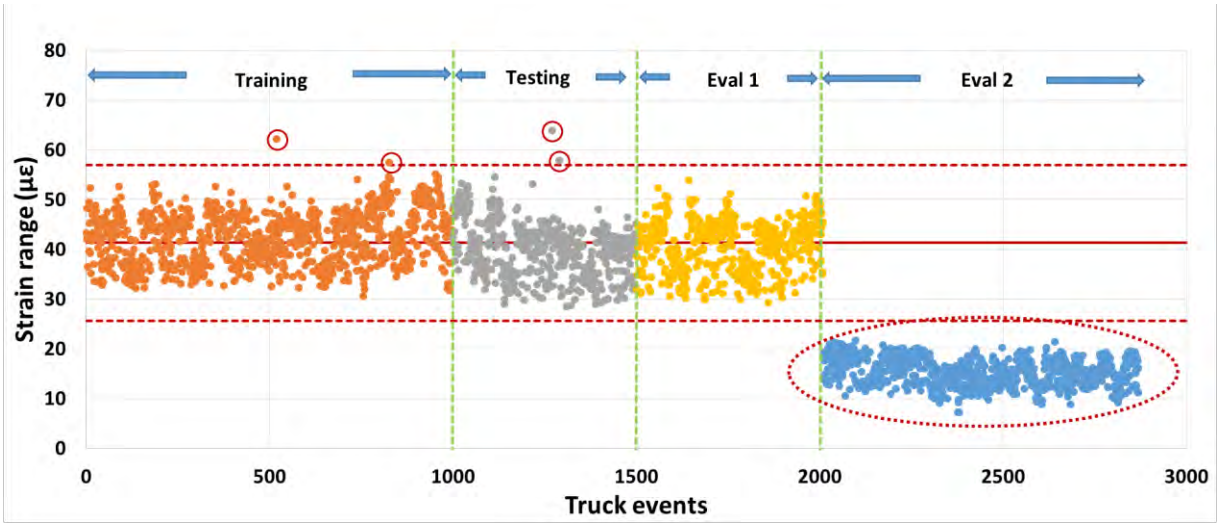

B-NG-BF-H

Figure 4.2. Example of false and true indication in a control chart

A true indication is defined as data points beyond the limits when there is truly damage. An example of true indication, in the dashed ellipse (lower right of the chart), is shown in Figure 4.2. After each specific damage-detection methodology is presented in this chapter, the methodology will be applied to cases of no damage and actual damage and evaluated with respect to damage-detection capability and with respect to false-indication rates.

4.2 Truck Event Control Chart Methods

4.2.1 Methodology

4.2.1.1 One-Truck Event Method

With the collected, filtered, and zeroed strain range data described in Section 4.1, control charts can be constructed directly using the strain range for each truck event for each sensor without further processing (i.e., one point on the control chart represents the strain range for a single truck event). These control charts would therefore represent the response data in their most basic form. In addition, in this form, a graphical representation is interpreted easily with fundamental structural engineering concepts. Control charts and associated limits are constructed using the mean and standard deviation of all trucks in the training period.

4.2.1.2 Truck Events Grouped by Ten Method

Group size can be an important parameter in constructing a control chart because it affects the control limits and the sensitivity of the false-indication rate. For example, the larger the group size, the narrower the control limits; therefore, slight damage could be detected from small variations (Lu et al. 2010). However, at the same time, larger group sizes increase the time that it takes for damage to be identified.

The optimal group size was previously determined to be 10 for this work (Lu 2008). Similar to the one-truck event approach, the mean of the means and standard deviations from data for 10 trucks (one group) are used as the chart variables. As before, the mean and standard deviations of the grouped strain range data during the training period are used to construct the control charts.

4.2.2 Select Results

The sensors listed in Table 4.2 will be used to illustrate the application of the truck event control chart methods for one-truck event (Section 4.2.1.1) and truck events grouped by ten (Section 4.2.1.2) below. These sensors were selected because they are typical of all results and they represent diverse sensor locations that include sensors on the bridge and on the sacrificial specimen.

Table 4.2. List of select sensors used to create sample control charts

Sensor Name
B-NG-BF-H
B-SG-BF-H
C-SG-BF-H
C-SG-CB(5)-V
C-SG-CB(4)-V
C-NG-BF-H
Sensor 1 on sacrificial specimen
Sensor 4 on sacrificial specimen

4.2.2.1 One-Truck Event Control Chart

Examples of one-truck event control charts for Specimen 2 for the selected sensors are shown in Figure 4.3. To establish the control limits for the various rules described in Section 4.1, the mean and standard deviation were calculated to be as shown in Table 4.3.

Table 4.3. Mean and standard deviations of select sensors for one-truck event method

Sensor name	Mean	Standard deviation
B-NG-BF-H	44	6
B-SG-BF-H	103	12
C-SG-BF-H	32	4
C-SG-CB(5)-V	92	11
C-SG-CB(4)-V	16	2
C-NG-BF-H	27	4
Sensor 1 on sacrificial specimen	100	15
Sensor 4 on sacrificial specimen	55	8

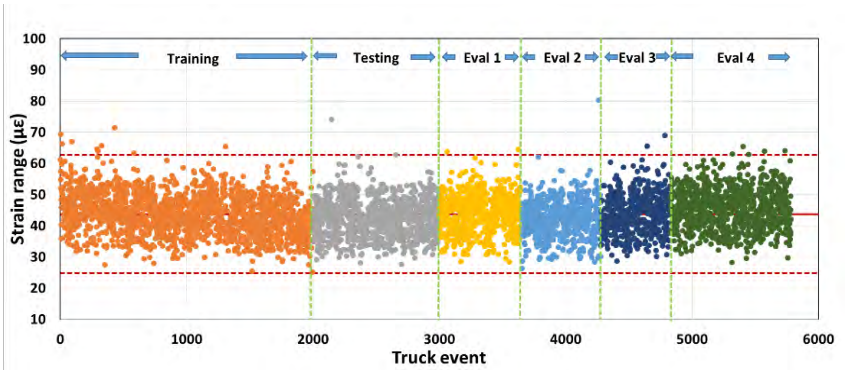

a. B-NG-BF-H

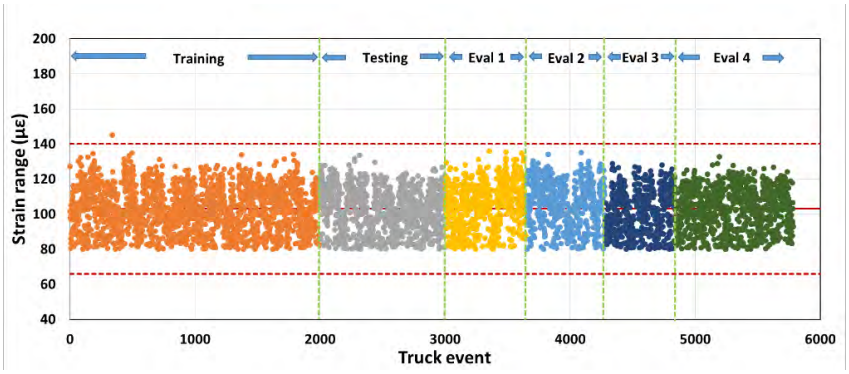

b. B-SG-BF-H

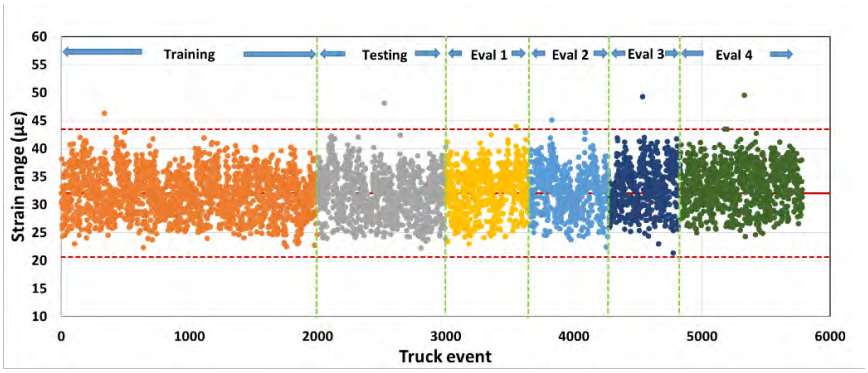

c. C-SG-BF-H

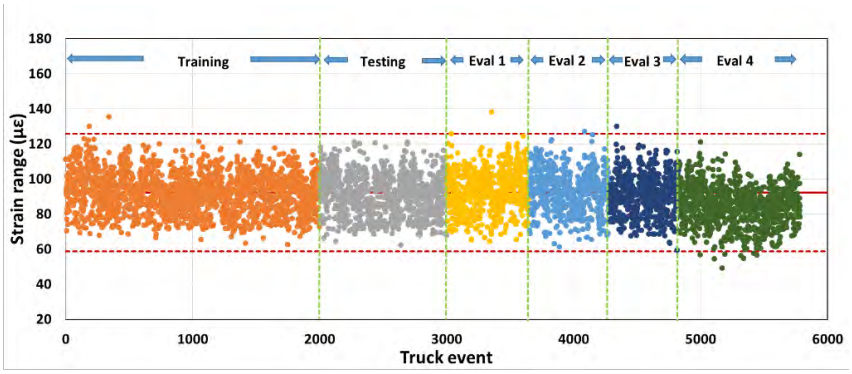

d. C-SG-CB(5)-V

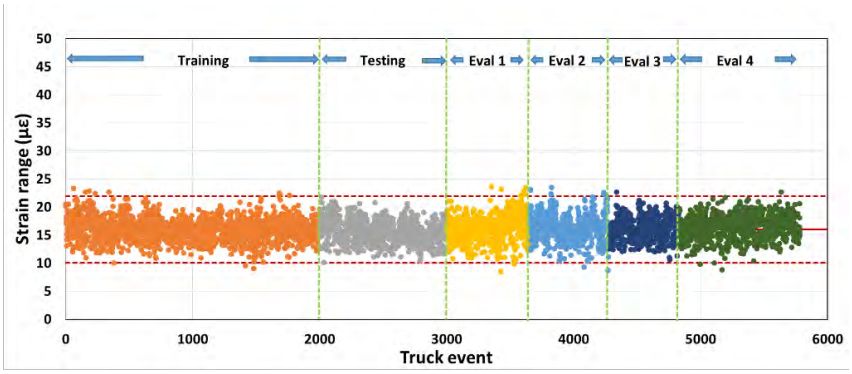

e. C-SG-CB(4)-V

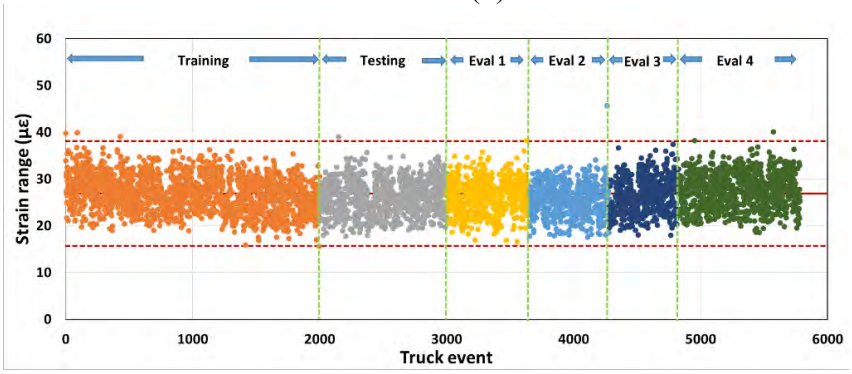

f. C-NG-BF-H

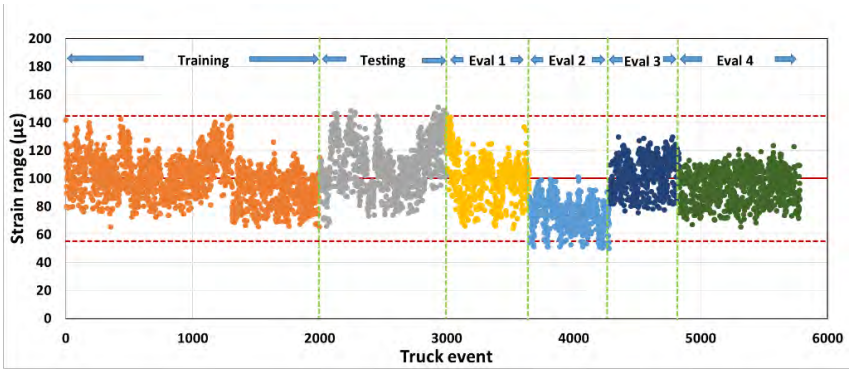

g. Sensor 1 on sacrificial specimen

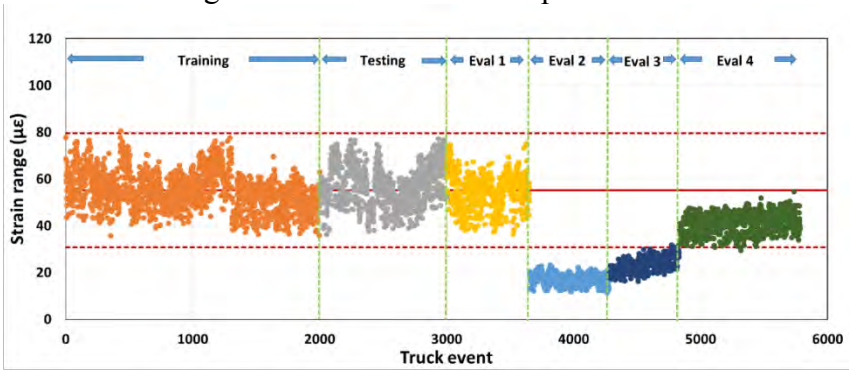

h. Sensor 4 on sacrificial specimen

Figure 4.3. One-truck event control charts for sacrificial Specimen 2

To summarize the propensity for violating the rules in Table 4.1, a table was developed to summarize the number of times that each rule was violated during each monitoring period. The rule violations for the one-truck event control chart method for select sensor are summarized in Table 4.4 and an additional table for all sensors is shown in Appendix A.

Table 4.4. Rule violations for one-truck event method

Sensor	Period	Rule 1	Rule 2	Rule 3	Rule 4	Rule 5	Rule 6	Total
B-NG-BF-H	Training	9	15	93	148	7	15	287
	Testing	2	2	42	82	5	7	140
	Evaluation 1	2		15	44	1		62
	Evaluation 2	1	4	35	62	2	1	105
	Evaluation 3	2	3	19	42	1	1	68
	Evaluation 4	5	6	22	45	3	2	83
	Total	21	30	226	423	19	26	745
	Rate (%)	0.4	0.5	3.9	7.3	0.3	0.5	2.1
B-SG-BF-H	Training	1	2	147	239	5	8	402
	Testing			88	172	2	5	267
	Evaluation 1		5	52	62	2	9	130
	Evaluation 2		2	88	133	4		227
	Evaluation 3			41	87	1		129
	Evaluation 4			40	79	5	5	129
	Total	1	9	456	772	19	27	1284
	Rate (%)	0.2	0.2	7.9	13.4	0.3	0.5	3.7
C-SG-BF-H	Training	1	17	123	138	5	11	295
	Testing	1	6	90	143	5	1	246
	Evaluation 1	1	3	38	78		6	126
	Evaluation 2	1	7	50	133	4		195
	Evaluation 3	1	9	56	40	6	3	115
	Evaluation 4	3		68	58	1		130
	Total	8	42	425	590	21	21	1107
	Rate (%)	0.1	0.7	7.4	10.2	0.4	0.4	3.2
C-SG-CB(5)-V	Training	2	15	76	129	2	16	240
	Testing		5	70	103	2	2	182
	Evaluation 1	2	8	18	47		7	82
	Evaluation 2	1	3	34	72	2	3	115
	Evaluation 3	1	4	42	43	1		91
	Evaluation 4	8	37	120	198	2	1	366
	Total	14	72	360	592	9	29	1076
	Rate (%)	0.2	1.2	6.2	10.3	0.2	0.5	3.10

Sensor	Period	Rule 1	Rule 2	Rule 3	Rule 4	Rule 5	Rule 6	Total
C-SG-CB(4)-V	Training	11	33	108	141	8	18	319
	Testing		12	77	189	2		280
	Evaluation 1	8	37	55	60	7		167
	Evaluation 2	9	33	96	111	9		258
	Evaluation 3	1	4	19	53	1	1	79
	Evaluation 4	4	4	50	89	1	2	150
	Total	33	123	405	643	28	21	1253
	Rate (%)	0.6	2.1	7.0	11.1	0.5	0.4	3.62
C-NG-BF-H	Training	4	18	137	242	9	3	413
	Testing	1	1	68	123	1	6	200
	Evaluation 1	1		39	47	1		88
	Evaluation 2	1	8	48	88	1		146
	Evaluation 3			37	69	3	3	112
	Evaluation 4	2	1	26	64	1		94
	Total	9	28	355	633	16	12	1053
	Rate (%)	0.2	0.5	6.2	11.0	0.3	0.2	3.0
Sensor 1 on sacrificial specimen	Training		46	311	451	8	8	824
	Testing	17	129	289	322	3	4	764
	Evaluation 1		23	100	161	2	4	290
	Evaluation 2	30	174	467	608	1		1280
	Evaluation 3			24	73	1	3	101
	Evaluation 4		1	43	103	1	1	149
	Total	47	373	1234	1718	16	20	3408
	Rate (%)	0.8	6.5	21.4	29.8	0.3	0.4	9.8
Sensor 4 on sacrificial specimen	Training	1	38	300	440	8	8	795
	Testing		25	207	193	4	1	430
	Evaluation 1		2	54	104	1	4	165
	Evaluation 2	627	625	623	620			2495
	Evaluation 3	549	549	547	544	1	3	2193
	Evaluation 4	1	181	821	945	3	8	1959
	Total	1178	1420	2552	2846	17	24	8037
	Rate (%)	20.4	24.6	44.2	49.3	0.3	0.4	23.2

Figure 4.3 and Table 4.4 show that during the training, testing, and Evaluation 1 periods (when there was no damage), there were a number of rule violations and the majority of those violations resulted from either Rule 3 or Rule 4. The rule violation rate for all sensors on the bridge were similar during all phases of monitoring indicating that the system was operating in a stable manner (also observable in Table 4.5). Once damage was introduced, the sensors on the specimen were collectively able to identify the damage with multiple rule violations of multiple types.

For each control chart region and each sensor, the number of rule violations and rate with respect to the six rules are counted and calculated by the automated software, BECAS, and are summarized in Table 4.4. The relatively high number of rule violations from Rule 3 and 4

significantly affect the overall false-indication rate. Table 4.5 shows the number of false indications for sensors on the bridge (non-damaged).

Table 4.5. Number of false indications for sensors on bridge (non-damaged) for one-truck event method

Sensor with no damage	False indications (Training, Testing, Evaluation 1, 2, 3, and 4)	False indication rate (%)
B-NG-BF-H	745	2.2
B-SG-BF-H	1284	3.7
C-SG-BF-H	1107	3.2
C-SG-CB(5)-V	1076	3.1
C-SG-CB(4)-V	1253	3.6
C-NG-BF-H	1053	3.0

When there was real damage near the sensors on the sacrificial specimen, the true-indication rate can be investigated by considering the Evaluation 2, 3, and 4 regions, which are summarized in Table 4.6. Note that, as expected, the true-indication rate is higher for Sensor 4 placed near the crack than for Sensor 1 placed away from the crack.

Table 4.6. Number of false and true indications for sensors on sacrificial specimen (near damage) for one-truck event method

Sensor near damage	False indications (Training, Testing, Evaluation 1)	False indication rate (%)	True indications (Evaluation 2, 3, and 4)	True indication rate (%)
Sensor 1	1878	8.6	1530	12.0
Sensor 4	1390	6.4	6647	52.2

4.2.2.2 Truck Events Grouped by Ten Control Chart

Examples of truck events grouped by ten control charts for Specimen 2 for select sensors are shown in Figure 4.4. The mean and standard deviation were calculated to establish the control limits for the various rules and are shown in Table 4.7. Note that the mean values are approximately the same as the one-truck event method but that the standard deviation is notably narrower because of the grouping process.

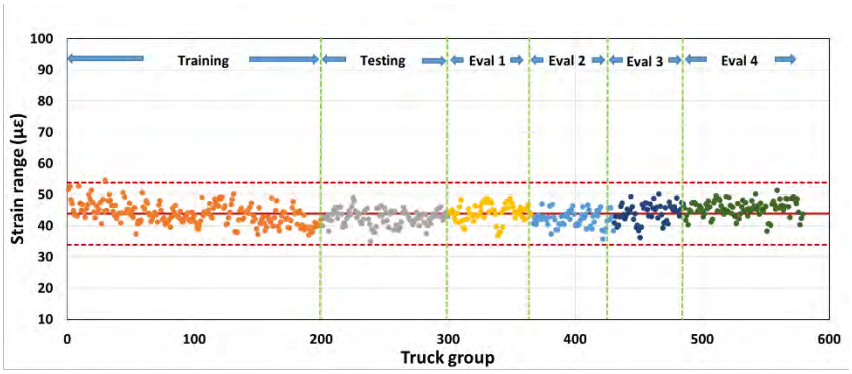

a. B-NG-BF-H

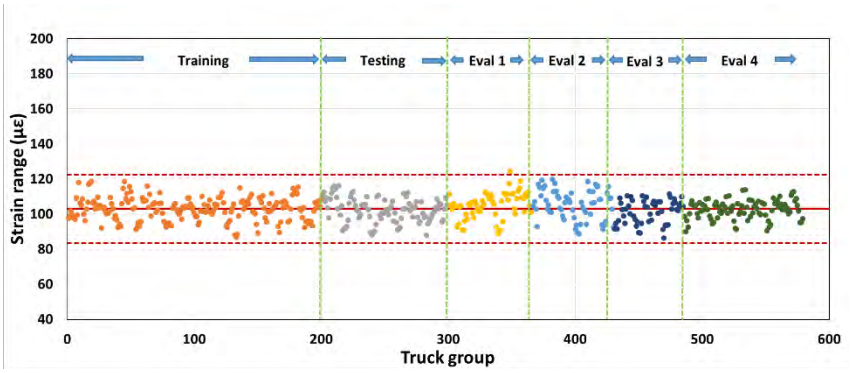

b. B-SG-BF-H

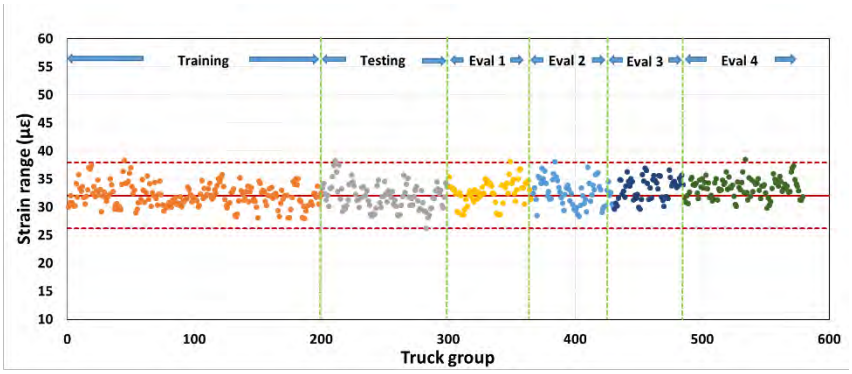

c. C-SG-BF-H

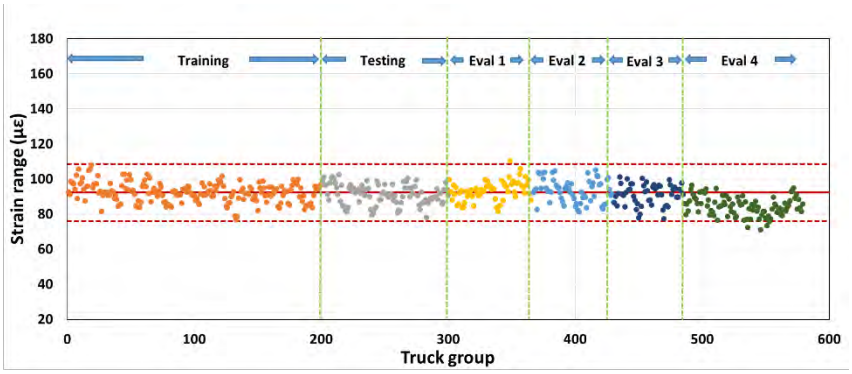

d. C-SG-CB(5)-V

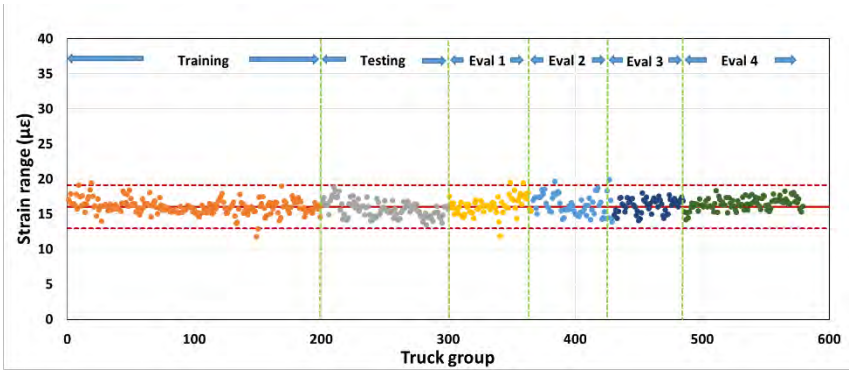

e. C-SG-CB(4)-V

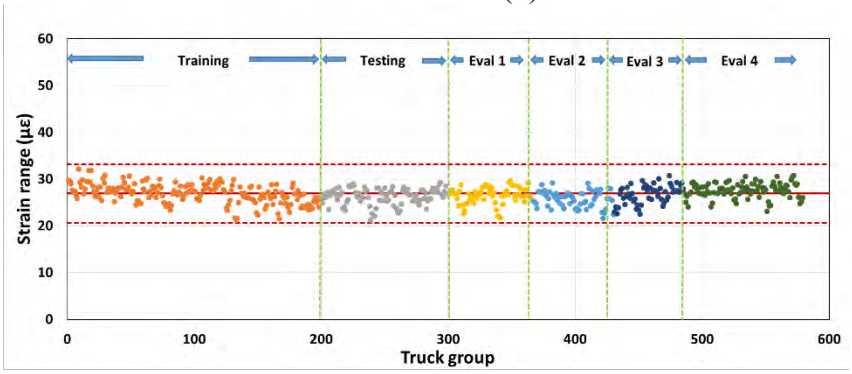

f. C-NG-BF-H

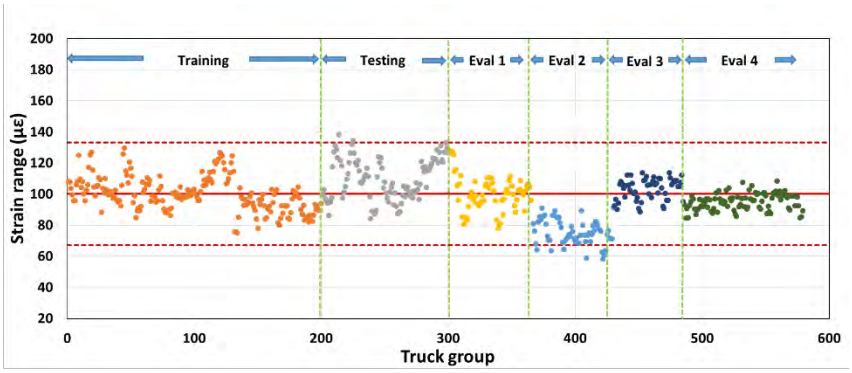

g. Sensor 1 on sacrificial specimen

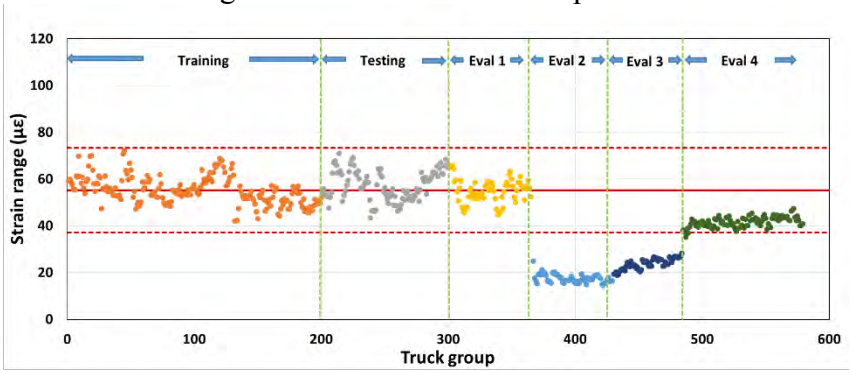

h. Sensor 4 on sacrificial specimen

Figure 4.4. Truck events grouped by ten control charts for sacrificial Specimen 2

Table 4.7. Mean and standard deviations of select sensors (με) for truck events grouped by ten method

Sensor name	Mean	Standard deviation
B-NG-BF-H	44	3
B-SG-BF-H	103	7
C-SG-BF-H	32	2
C-SG-CB(5)-V	92	6
C-SG-CB(4)-V	16	1
C-NG-BF-H	27	2
Sensor 1 on sacrificial specimen	100	11
Sensor 4 on sacrificial specimen	56	6

As with the one-truck event methodology, a table was constructed to summarize the tendency for violating the control chart rules. From Figure 4.4 and Table 4.8, it is observed that during the training, testing, and Evaluation 1 periods (when there was no damage), there were a number of rule violations and that the majority of those resulted from either Rule 3 or Rule 4.

From Figure 4.4, sensors on the bridge (non-damaged) follow control chart Rule 1 well. It was also found that sensors near damage (i.e., Sensor 4) show violations of Rule 1 in the Evaluation 2, 3, and 4 regions. In Table 4.8, the methodology found significantly high numbers of rule violations from Rule 3 and Rule 4 and those violations affect the overall false-indication rate significantly.

Table 4.8. Rule violations for truck events grouped by ten method

Sensor	Period	Rule 1	Rule 2	Rule 3	Rule 4	Rule 5	Rule 6	Total
B-NG-BF-H	Training	1	1	21	18	4		45
	Testing			12	10	3		25
	Evaluation 1			9	3	2		14
	Evaluation 2		2	6	1			9
	Evaluation 3			6	6			12
	Evaluation 4			6	13			19
	Total	1	3	60	51	9	0	124
	Rate (%)	0.2	0.5	10.5	9.0	1.6	0	3.61
B-SG-BF-H	Training		6	36	7	4		53
	Testing		3	22	5	11		41
	Evaluation 1	1	2	12	6	2		23
	Evaluation 2		6	17	3	3		29
	Evaluation 3		2	14		3		19
	Evaluation 4			9				9
	Total	1	19	110	21	23	0	174
	Rate (%)	0.2	3.3	19.2	3.7	4.0	0	5.07

Sensor	Period	Rule 1	Rule 2	Rule 3	Rule 4	Rule 5	Rule 6	Total
C-SG-BF-H	Training	1	9	19	22	4		55
	Testing	1	6	21	5	3		36
	Evaluation 1	1	2	12	6	3		24
	Evaluation 2	2	4	13	3	1		23
	Evaluation 3		2	12	7	1		22
	Evaluation 4	1	4	13	22	2		42
	Total	6	27	90	65	14	0	202
	Rate (%)	1.0	4.7	15.7	11.4	2.5	0	5.89
C-SG-CB(5)-V	Training		6	29	12	6		53
	Testing		2	17	5			24
	Evaluation 1	1		6	6			13
	Evaluation 2			14	6	3		23
	Evaluation 3		4	10				14
	Evaluation 4	4	23	53	51	3		134
	Total	5	35	129	80	12	0	261
	Rate (%)	0.9	6.1	22.5	14.0	2.1	0	7.60
C-SG-CB(4)-V	Training	4	6	9	16	4		39
	Testing		2	34	10	1		47
	Evaluation 1	3	2	9	2			16
	Evaluation 2	4	10	10	2	2		28
	Evaluation 3			2				2
	Evaluation 4			1	17			18
	Total	11	20	65	47	7	0	150
	Rate (%)	1.9	3.5	11.3	8.3	1.2	0	4.37
C-NG-BF-H	Training		6	29	31	7	3	76
	Testing		4	14	4	1		23
	Evaluation 1		3	8	4	2		17
	Evaluation 2		2	10	5			17
	Evaluation 3			9	1			10
	Evaluation 4			1	9			10
	Total	0	15	71	54	10	3	153
	Rate (%)	0	2.6	12.4	9.8	1.8	0.5	4.46
Sensor 1 on sacrificial specimen	Training		11	35	48	5		99
	Testing	2	20	41	31	7		101
	Evaluation 1		3	11	2	2		18
	Evaluation 2	7	39	56	55	1		158
	Evaluation 3				10			10
	Evaluation 4			3	29			32
	Total	9	73	146	175	15	0	418
	Rate (%)	1.6	12.7	25.5	30.7	2.6	0	12.18

Sensor	Period	Rule 1	Rule 2	Rule 3	Rule 4	Rule 5	Rule 6	Total
Sensor 4 on sacrificial specimen	Training		10	30	67	5		112
	Testing		2	33	33	7		75
	Evaluation 1			9	2	1		12
	Evaluation 2	62	60	58	55	2		237
	Evaluation 3	55	53	51	48			207
	Evaluation 4	2	72	91	88			253
	Total	119	197	272	293	15	0	896
	Rate (%)	20.6	34.3	47.5	51.4	2.6	0	26.1

Tables 4.9 and 4.10 summarize the number of false indications for sensors on the bridge (non-damaged) and the number of false and true indications for sensors on the specimen (near damage). It was found that the true-indication rate is similar to the one-truck event method.

Table 4.9. Number of false indications for sensors on bridge (non-damaged) for truck events grouped by ten method

Sensor with no damage	False indications (Training, Testing, Evaluation 1, 2, 3, and 4)	False indication rate (%)
B-NG-BF-H	124	3.6
B-SG-BF-H	174	5.1
C-SG-BF-H	202	5.9
C-SG-CB(5)-V	261	7.9
C-SG-CB(4)-V	150	4.4
C-NG-BF-H	153	4.5

Table 4.10. Number of false and true indications for sensors on sacrificial specimen (near damage) for truck events grouped by ten method

Sensor near damage	False indications (Training, Testing, Evaluation 1)	False indication rate (%)	True indications (Evaluation 2, 3, and 4)	True indication rate (%)
Sensor 1	218	10.4	200	16.1
Sensor 4	199	9.2	697	56.1

4.3 Cross Prediction Control Chart Method

4.3.1 Methodology

Fundamentally, the cross prediction method presented here is an adaptation of the method described in Chapter 2. The primary differences in the methodology are the use of orthogonal

regression and the simplification approach. Like the method presented in Chapter 2, truck events are grouped into a group size of 10. A general flow chart for the method is shown in Figure 4.5.

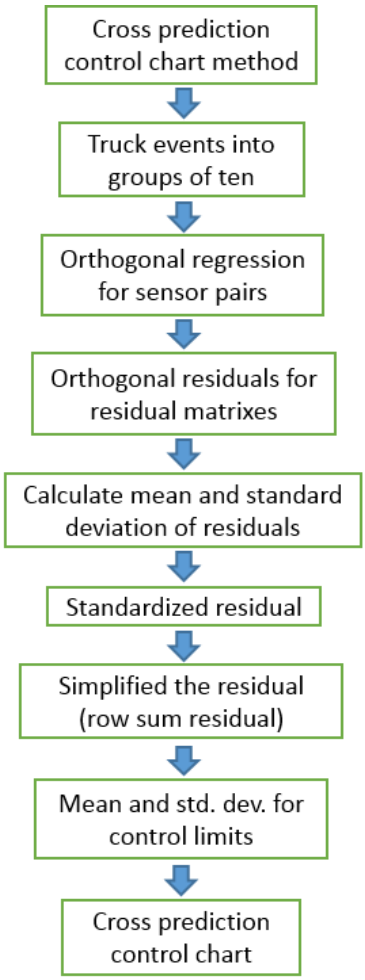

Figure 4.5. Cross prediction method flow chart

During training, orthogonal regression as described in Section 2.3.1 is performed for every combination of sensor pairs, ε_i and ε_j, where i and j range from 1 to q (number of sensors). Because orthogonal regression is used, the relationship between ε_i and ε_j is the inverse of the relationship between ε_j and ε_i. Orthogonal residuals are then calculated as previously discussed in Section 2.3.1 and assembled into residual matrixes (q by q) for each truck group with p (number of groups) of these matrices.

$$[r_g] = \begin{bmatrix} r11 & \cdots & r1q \\ \vdots & rij & \vdots \\ rq1 & \cdots & rqq \end{bmatrix} \quad \textbf{(4-1)}$$

Standardizing the residuals are helpful to normalize the residual values that vary over a large range of values (Lu 2008). The process for standardizing the residual for all sensor pairs for each truck group is given in Equations 4-2 and 4-3:

$$z_{ij} = \frac{r_{ij} - \overline{r}_{ij}}{s_{ij}} \quad \textbf{(4-2)}$$

$$[\overline{r}] = \begin{bmatrix} \overline{r}_{11} & \cdots & \overline{r}_{1q} \\ \vdots & \overline{r}_{ij} & \vdots \\ \overline{r}_{q1} & \cdots & \overline{r}_{qq} \end{bmatrix} \qquad [s] = \begin{bmatrix} s_{11} & \cdots & s_{1q} \\ \vdots & s_{ij} & \vdots \\ s_{q1} & \cdots & s_{qq} \end{bmatrix} \quad \textbf{(4-3)}$$

where $\overline{r}_{ij}$ is the average of r_{ij} for all the groups and s_{ij} is the standard deviation. This process results in another set of q by q standardized-residual matrices and there are p of these, with one for each group.

$$[z_g] = \begin{bmatrix} z_{11} & \cdots & z_{1q} \\ \vdots & z_{ij} & \vdots \\ z_{q1} & \cdots & z_{qq} \end{bmatrix} \quad \textbf{(4-4)}$$

To further simply the standardized-residual data to a single control chart for each sensor, the standardized residual matrix $[Z_g]$ is reduced to a set of p simplified residual vectors $[R]$ by summing each row.

$$R_i = row\ sum_i = \sum_{j=1}^{q} z_{ij} \quad \textbf{(4-5)}$$

$$[R] = \begin{bmatrix} R_1 \\ \vdots \\ R_i \\ \vdots \\ R_q \end{bmatrix} \quad \textbf{(4-6)}$$

The mean and standard deviation of the $[R]$ residuals for all training truck groups are calculated and then used to set control limits.

$$[\overline{R}] = \begin{bmatrix} \overline{R}_1 \\ \vdots \\ \overline{R}_i \\ \vdots \\ \overline{R}_q \end{bmatrix} \qquad [S] = \begin{bmatrix} S_1 \\ \vdots \\ S_i \\ \vdots \\ S_q \end{bmatrix} \quad \textbf{(4-7)}$$

For each group of 10 truck events occurring during subsequent monitoring, an orthogonal residual matrix is obtained by using the orthogonal regression from the training period (Equation 4-1). The mean and standard deviation of the standardized residual (Equation 4-2) from the

training period are again used to calculate the standardized residuals (Equation 4-4) and, after the residual-simplification process, a point R_i for this group is plotted on each control chart.

4.3.2 Select Results

With the cross prediction method, the average of the standardized residuals are always equal to zero due to the standardization process. As was mentioned previously, the standard deviations are used to establish control limits that are applied to the various rules. Table 4.11 shows the mean and standard deviations of select sensors. As can be seen in Table 4.11, there was a fair amount of consistency in the standard deviations indicating that the standardization process was effective at reducing large ranges of residual values.

Table 4.11. Mean and standard deviations of selected sensors (με) for cross prediction method

Sensor name	Mean	Standard deviation
B-NG-BF-H	0	25
B-SG-BF-H	0	21
C-SG-BF-H	0	29
C-SG-CB(5)-V	0	19
C-SG-CB(4)-V	0	34
C-NG-BF-H	0	28
Sensor 1 on sacrificial specimen	0	26
Sensor 4 on sacrificial specimen	0	25

In Figure 4.6, R-sum values for global response sensors on the bridge (non-damaged) follow Rule 1 well, as data points are generally within the plus/minus three standard deviation limits. However, there are a large number of false indications (Rule 1) for sensors placed in the web cut-back region of the bridge (Sensors C-SG-CB(5)-V and C-SG-CB(4)-V). In Figure 4.6h, for example, it would be inferred that there is damage because the R-sum values exceed the limits for Rule 1 in the Evaluation 2, 3, and 4 regions.

The number of rule violations and rate with respect to all rules were determined and are shown in Table 4.12. A large number of rule violations are found for Rule 3 or Rule 4 as was the case with the strain range methods.

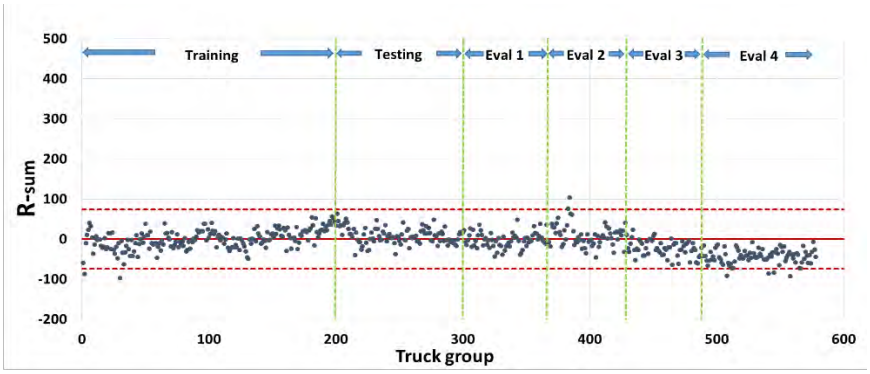

a. B-NG-BF-H

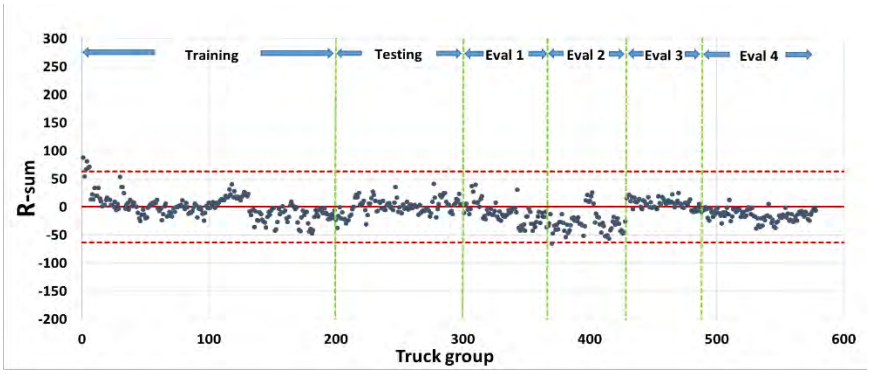

b. B-SG-BF-H

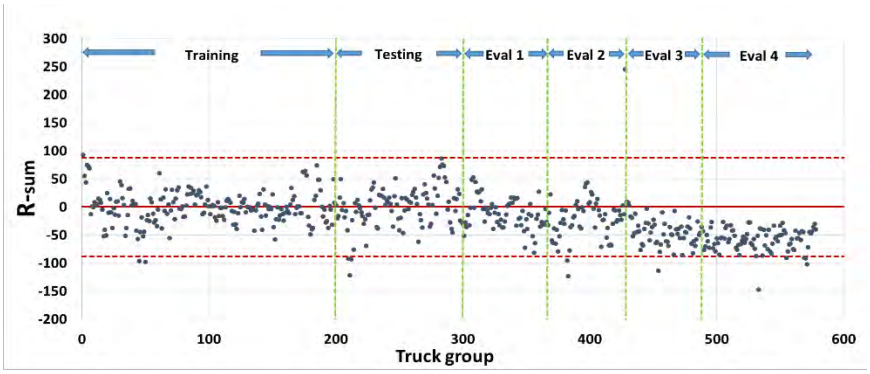

c. C-SG-BF-H

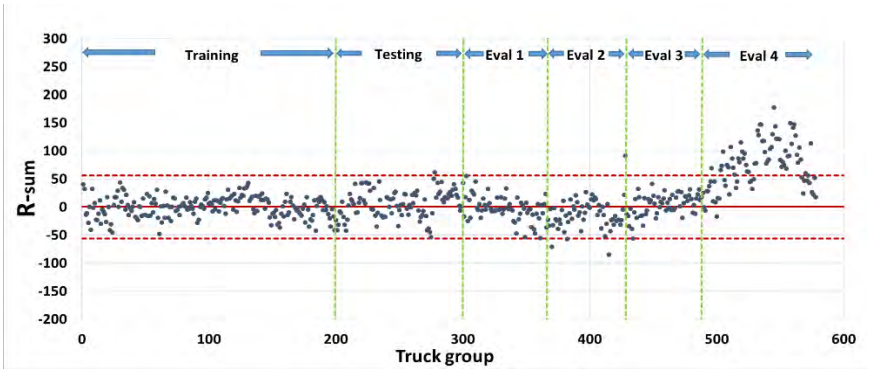

d. C-SG-CB(5)-V

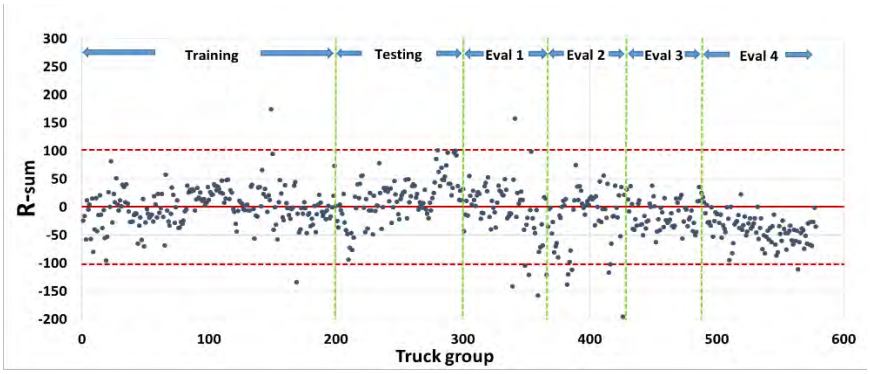

e. C-SG-CB(4)-V

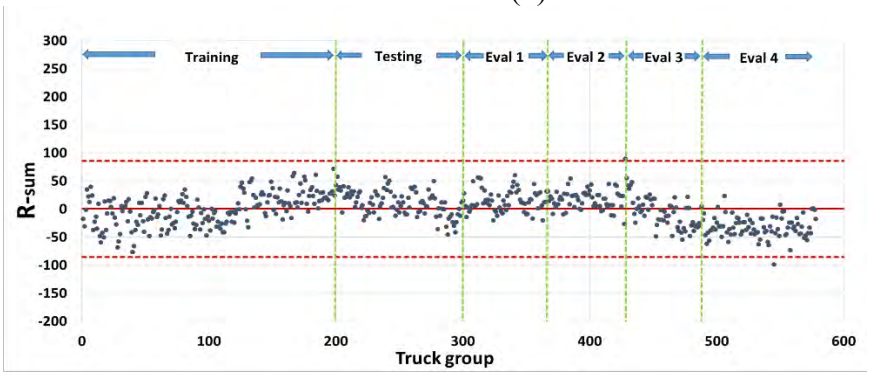

f. C-NG-BF-H

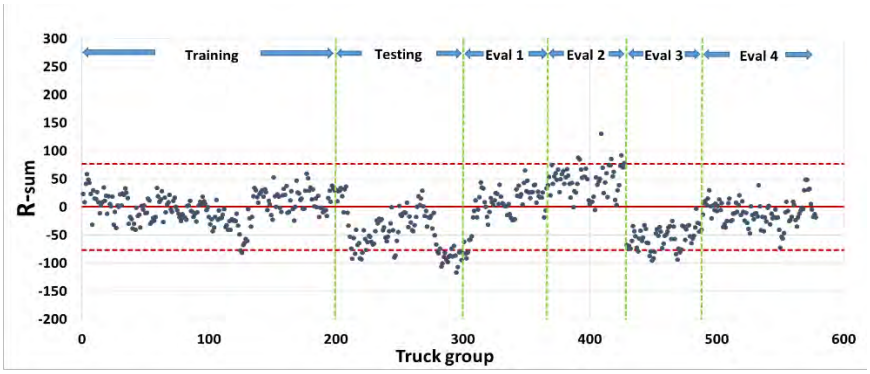

g. Sensor 1 on sacrificial specimen

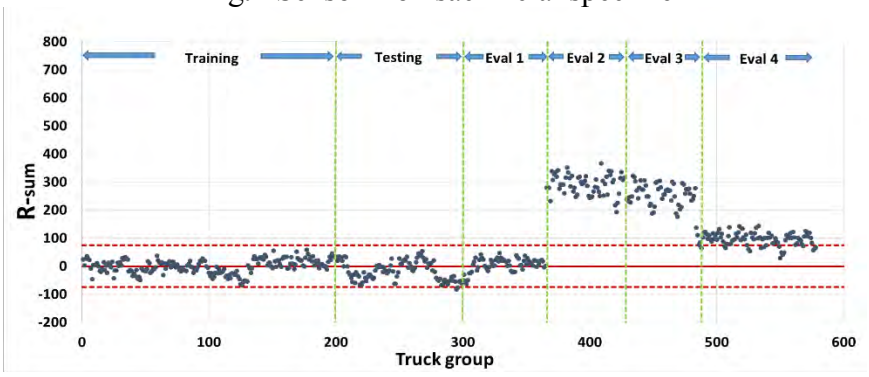

h. Sensor 4 on sacrificial specimen

Figure 4.6. Cross prediction control charts for sacrificial Specimen 2

Table 4.12. Rule violations for cross prediction method

Sensor	Period	Rule 1	Rule 2	Rule 3	Rule 4	Rule 5	Rule 6	Total
B-NG-BF-H	Training	2	3	14	31	2		52
	Testing			8	11	1		20
	Evaluation 1			2				2
	Evaluation 2	2	4	5	3			14
	Evaluation 3			4	22			26
	Evaluation 4	4	24	70	88			186
	Total	8	31	103	155	3	0	300
	Rate (%)	1.4	5.4	18.0	27.2	0.5	0.0	8.7
B-SG-BF-H	Training	5	6	21	87	5		124
	Testing			5	13	5		23
	Evaluation 1			10	29			39
	Evaluation 2	1	10	36	42			89
	Evaluation 3				6			6
	Evaluation 4			7	69			76
	Total	6	16	79	246	10	0	357
	Rate (%)	1.0	2.8	13.8	43.2	1.8	0.0	10.4
C-SG-BF-H	Training	3	6	22	13	2		46
	Testing	3	8	11	6	4		32
	Evaluation 1		2	3	6	2		13
	Evaluation 2	3	10	20	24	3		60
	Evaluation 3	1	14	37	45	1		98
	Evaluation 4	5	41	85	88			219
	Total	15	81	178	182	12	0	468
	Rate (%)	2.6	14.1	31.1	31.9	2.1	0.0	13.6
C-SG-CB(5)-V	Training		1	12	11			24
	Testing	1	12	19	17	2		51
	Evaluation 1		2	4	1	1		8
	Evaluation 2	4	3	17	11			35
	Evaluation 3	1	2					3
	Evaluation 4	59	76	77	72	2		286
	Total	65	96	129	112	5	0	407
	Rate (%)	11.3	16.7	22.5	19.7	0.9	0.0	11.9
C-SG-CB(4)-V	Training	2	2	5	27	1		37
	Testing		10	25	20	2		57
	Evaluation 1	5	4	2	5			16
	Evaluation 2	8	10	12	5	1		36
	Evaluation 3			2	5			7
	Evaluation 4	1	4	34	55	1		95
	Total	16	30	80	117	5	0	248
	Rate (%)	2.8	5.2	14.0	20.5	0.9	0.00	7.2

Sensor	Period	Rule 1	Rule 2	Rule 3	Rule 4	Rule 5	Rule 6	Total
C-NG-BF-H	Training		6	16	41	1		64
	Testing			11	18	1		30
	Evaluation 1			9	16	1		26
	Evaluation 2	1			12	1		14
	Evaluation 3			7	4			11
	Evaluation 4	1	2	37	58			98
	Total	2	8	80	149	4	0	243
	Rate (%)	0.4	1.4	14.0	26.1	0.7	0.0	7.08
Sensor 1 on sacrificial specimen	Training	2	6	21	32	1	1	63
	Testing	25	47	59	58	1		190
	Evaluation 1	3	6	15	23	5		52
	Evaluation 2	7	30	42	39			118
	Evaluation 3	9	31	50	48	2		140
	Evaluation 4		3	16	6			25
	Total	46	123	203	206	9	1	588
	Rate (%)	8.0	21.4	35.4	36.1	1.6	0.2	17.1
Sensor 4 on sacrificial specimen	Training		6	31	47	6	1	91
	Testing	2	23	43	35	2		105
	Evaluation 1		3	5	12	2		22
	Evaluation 2	63	61	59	55	1		239
	Evaluation 3	55	53	51	48			207
	Evaluation 4	79	89	91	88			347
	Total	199	235	280	285	11	1	1011
	Rate (%)	34.4	40.9	48.9	50.0	1.9	0.2	29.5

Tables 4.13 and 4.14 show the number of false indications for sensors on the bridge (non-damaged) and on the sacrificial specimen (near damage), respectively. It was also found that the cross prediction method had a higher true-indication rate than either of the strain range methods.

Table 4.13. Number of false indications for sensors on bridge (non-damaged) for cross prediction method

Sensor with no damage	False indications (Training, Testing, Evaluation 1, 2, 3, and 4)	False indication rate (%)
B-NG-BF-H	300	8.7
B-SG-BF-H	357	10.4
C-SG-BF-H	468	13.6
C-SG-CB(5)-V	407	11.9
C-SG-CB(4)-V	248	7.2
C-NG-BF-H	243	7.1

Table 4.14. Number of false and true indications for sensors on sacrificial specimen (near damage) for cross prediction method

Sensor near damage	False indications (Training, Testing, Evaluation 1)	False indication rate (%)	True indications (Evaluation 2, 3, and 4)	True indication rate (%)
Sensor 1	305	14.2	283	22.8
Sensor 4	218	10.1	793	63.9

4.4 F-Test Control Chart Method

4.4.1 F_{shm} Method

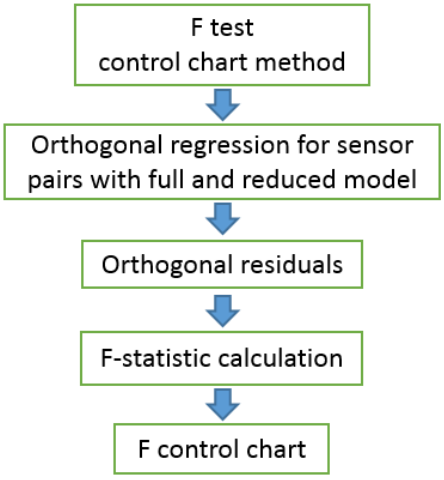

Figure 4.7. Flow chart for F_{shm} control chart method

A statistical test known as the f-test was described in Section 2.3.2. Here, a damage detection approach known as the F_{shm} method is presented and discussed. The F_{shm} method is loosely based on f-test concepts. The primary difference between the f-test and F_{shm} method is that the f-test required that traditional linear regression be used. The F_{shm} approach utilizes the more appropriate orthogonal regression described previously. The f-test has been further expanded by the F_{shm} approach to include control chart concepts such that condition can be tracked with time.

$$Fshm = \frac{SSRreduced - SSRfull}{dfreduced - dffull} \div \frac{SSR\,full}{dffull} \quad \textbf{(4-8)}$$

In constructing the F_{shm} control chart, the first 200 truck events recorded during training have been designated as the baseline data. These data will be the point of comparison for all subsequent evaluation.

For trucks from 201 through 2,000, groups of 200 trucks (with 150 trucks overlapping between groups) are compared against the baseline data using the F_{shm} equation. This ensures that all F_{shm} values have the same sample size (200 are from the baseline data and another 200 are for comparison). Collectively, this series of F_{shm} values are then used to establish the mean and standard deviations for all such evaluations made during the training period (up through truck number 2,000). The means and standard deviations then establish the control chart limits by which the various tests will be evaluated.

With this approach, the data are evaluated via sensor pairings, much like the early portion of the cross prediction methodology. However, unlike the cross prediction method, no simplification is made and, therefore, $(n^2-n)/2$ evaluations are made. This results in a very large number of evaluations being made after each successive passage of 50 trucks.

4.4.2 Select Results

To study the F_{shm} approach, 12 sensor pairs were selected and the mean and standard deviation from the training period were calculated (listed in Table 4.15) as described in the previous section. As expected, high F_{shm} values resulted for sensor pairs that included a sensor on the sacrificial specimen during the Evaluation 2, 3, and 4 periods indicating that damage was readily detected.

Table 4.15. Mean and standard deviations of select sensors (με) for F_{shm} method

Sensor pairs	Mean	Standard deviation
B-NG-BF-H vs. B-SG-BF-H	18	13
B-NG-BF-H vs. C-SG-BF-H	4	3
B-NG-BF-H vs. C-SG-CB(5)-V	6	6
B-NG-BF-H vs. C-SG-CB(4)-V	6	6
B-SG-BF-H vs. C-NG-BF-H	30	27
C-SG-BF-H vs. C-NG-BF-H	17	12
C-SG-CB(5)-V vs. C-SG-CB(4)-V	8	11
C-SG-CB(5)-V vs. C-NG-BF-H	9	11
C-SG-CB(4)-V vs. C-NG-BF-H	9	9
B-NG-BF-H vs. Sensor 4	23	14
B-SG-BF-H vs. Sensor 1	89	84
B-SG-BF-H vs. Sensor 4	149	136

As Table 4.16 shows, no rule violations were found for Rules 6 or 3 and Rule 4 had many rule violations as was observed for the other methodologies.

Table 4.16. Rule violations for F_{shm} control chart

Sensor pairs	Period	Rule 1	Rule 2	Rule 3	Rule 4	Rule 5	Rule 6	Total
B-NG-BF-H	Training		2	9	14	4		29
vs.	Testing	2	2	1	5	2		12
B-SG-BF-H	Evaluation 1		1	1	5	1		8
	Evaluation 2	2	7	3	8			20
	Evaluation 3			4	4	6		14
	Evaluation 4			11	19			30
	Total	4	12	29	55	13	0	113
	Rate (%)	3.7	11.4	28.2	55.0	12.8	0.0	18.5
B-NG-BF-H	Training			3	1	2		6
vs.	Testing	4	4	2	2	2		14
C-SG-BF-H	Evaluation 1	2	4	6	1	1		14
	Evaluation 2	6	8	3	6			23
	Evaluation 3	4	8	9	7			28
	Evaluation 4	2	3	4	19			28
	Total	18	27	27	36	5	0	113
	Rate (%)	16.7	25.7	26.2	36.0	4.9	0.0	18.5
B-NG-BF-H	Training	1	2	5	13	1		22
vs.	Testing	3	2	1	5	2		13
C-SG-CB(5)-H	Evaluation 1		1	2	1	3		7
	Evaluation 2	3	7	5	3	2		20
	Evaluation 3				1	2		3
	Evaluation 4		1	4	12	2		19
	Total	7	13	17	35	12	0	84
	Rate (%)	6.5	12.4	16.5	35.0	11.8	0.0	13.7
B-NG-BF-H	Training			6	7	23		36
vs.	Testing	2	2	2	11	1		18
C-SG-CB(4)-V	Evaluation 1			1				1
	Evaluation 2				11			11
	Evaluation 3							0
	Evaluation 4				10			10
	Total	2	2	9	39	24	0	76
	Rate (%)	1.9	1.9	8.7	39.0	23.5	0.0	12.4
B-SG-BF-H	Training		1	10	4			15
vs.	Testing	2	1	7	2			12
C-NG-BF-H	Evaluation 1			5	4			9
	Evaluation 2		6	10	11	1		28
	Evaluation 3				5	6		11
	Evaluation 4				18	2		20
	Total	2	8	32	44	9	0	95
	Rate (%)	1.9	7.6	31.1	44.0	8.8	0.0	15.52

Sensor pairs	Period	Rule 1	Rule 2	Rule 3	Rule 4	Rule 5	Rule 6	Total
C-SG-BF-H	Training			13	14	5		32
vs.	Testing	4	4	4	16	1		29
C-NG-BF-H	Evaluation 1	1	6	8	5	2		22
	Evaluation 2	8	9	11	11			39
	Evaluation 3	7	7	11	11	2		38
	Evaluation 4			3	19	1		23
	Total	20	26	50	76	11	0	183
	Rate (%)	18.5	24.8	48.5	76.0	10.8	0.0	29.9
C-SG-CB(5)-V	Training		3	3	3	4		13
vs.	Testing	1	5	6	5	4		21
C-SG-CB(4)-V	Evaluation 1				2	1		3
	Evaluation 2				9			9
	Evaluation 3				11	1		12
	Evaluation 4	13	12	11	12	3		51
	Total	14	20	20	42	13	0	109
	Rate (%)	13.0	19.1	19.4	42.0	12.8	0.0	17.8
C-SG-CB(5)-V	Training		2	5	23			30
vs.	Testing	2	3	1	7	1		14
C-NG-BF-H	Evaluation 1		1	5		1		7
	Evaluation 2	1	7	11	11	1		31
	Evaluation 3		1	1	5	2		9
	Evaluation 4			3	11	5		19
	Total	3	14	26	57	10	0	110
	Rate (%)	2.8	13.3	25.2	57.0	9.8	0.0	18.0
C-SG-CB(4)-V	Training		2	4	10	5		21
vs.	Testing	2	2		7			11
C-NG-BF-H	Evaluation 1				2	1		3
	Evaluation 2							0
	Evaluation 3				11	1		12
	Evaluation 4				19	2		21
	Total	2	4	4	49	9	0	68
	Rate (%)	1.9	3.8	3.9	49.0	8.8	0.0	11.1
B-NG-BF-H	Training			6	5	1		12
vs.	Testing	1	3	7		3		14
Sensor 1 on	Evaluation 1	2	3	2				7
sacrificial	Evaluation 2	11	11	11	5	3		41
specimen	Evaluation 3	11	11	11	11			44
	Evaluation 4	19	17	15	19			70
	Total	44	45	52	40	7	0	188
	Rate (%)	40.7	42.9	50.5	40.0	6.9	0.0	30.7

Sensor pairs	Period	Rule 1	Rule 2	Rule 3	Rule 4	Rule 5	Rule 6	Total
B-SG-BF-H vs. Sensor 1 on sacrificial specimen	Training			7	19	3		29
	Testing	1	2	6		3		12
	Evaluation 1			1		2		3
	Evaluation 2	9	10	9	9			37
	Evaluation 3			8	4	3		15
	Evaluation 4				7			7
	Total	10	12	31	39	11	0	103
	Rate (%)	9.3	11.4	30.1	39.0	10.8	0.0	16.8
B-SG-BF-H vs. Sensor 4 on sacrificial specimen	Training			9	23	1		33
	Testing			1	6	4		11
	Evaluation 1				4			4
	Evaluation 2	9	10	10	11			40
	Evaluation 3	11	11	11	11			44
	Evaluation 4	19	17	15	19			70
	Total	39	38	46	74	5	0	202
	Rate (%)	36.1	36.2	44.7	74.0	4.9	0.0	15.9

In Figure 4.8, F_{shm} values for global response sensors on the bridge (non-damaged) follow Rule 1 well, as data points are generally within the plus/minus three standard deviation limits. However, as with the cross prediction method, there are a large number of false indications (Rule 1) for sensors placed in the web cut-back region of the bridge (Sensors C-SG-CB(5)-V and C-SG-CB(4)-V).

The number of rule violations and rates with respect to all rules were determined and are shown in Table 4.16. A large number of rule violations are found for Rule 3 or Rule 4, as was the case with the strain range methods and the cross prediction method.

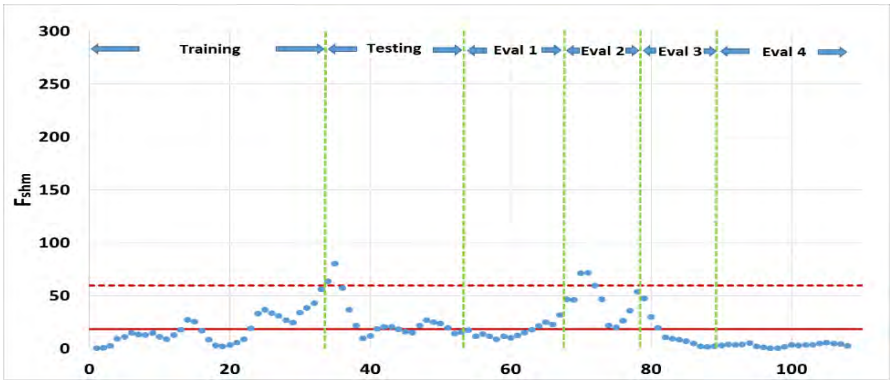

a. B-NG-BF-H vs. B-SG-BF-H

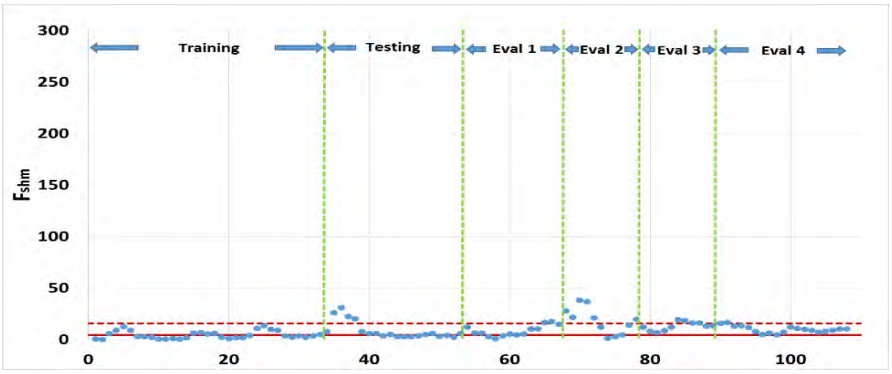

b. B-NG-BF-H vs. C-SG-BF-H

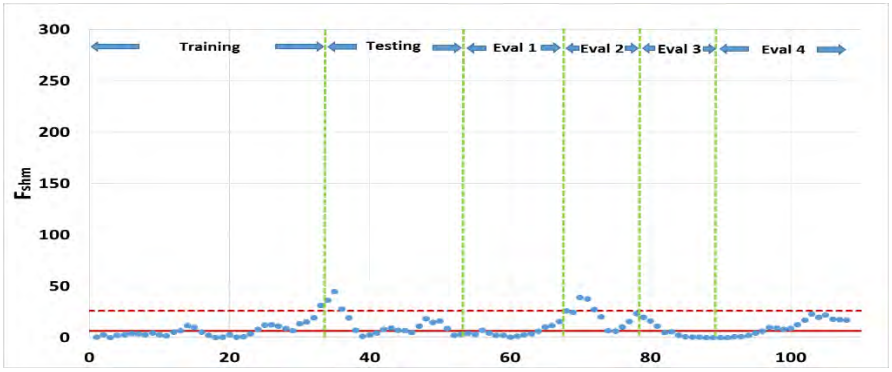

c. B-NG-BF-H vs. C-SG-SB(5)-H

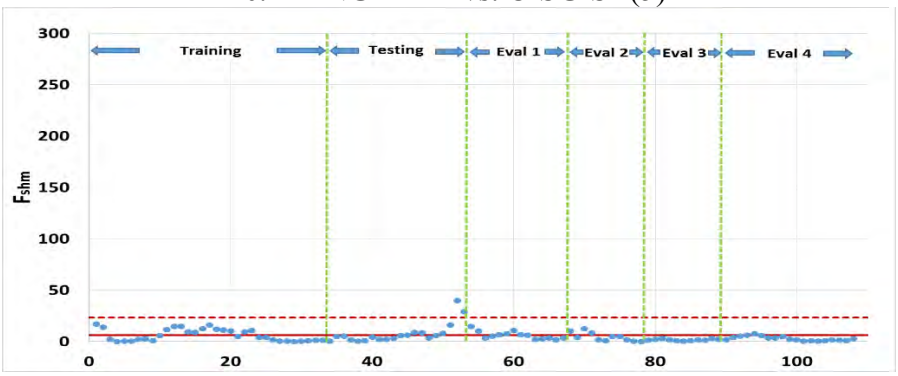

d. B-NG-BF-H vs. C-SG-CB(4)-V

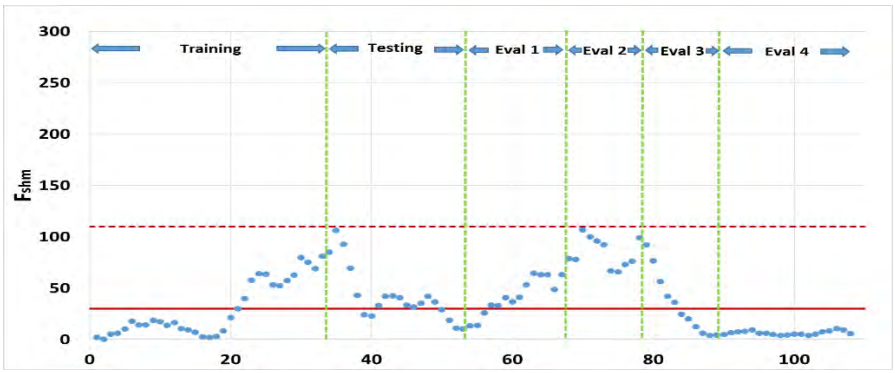

e. B-SG-BF-H vs. C-NG-BF-H

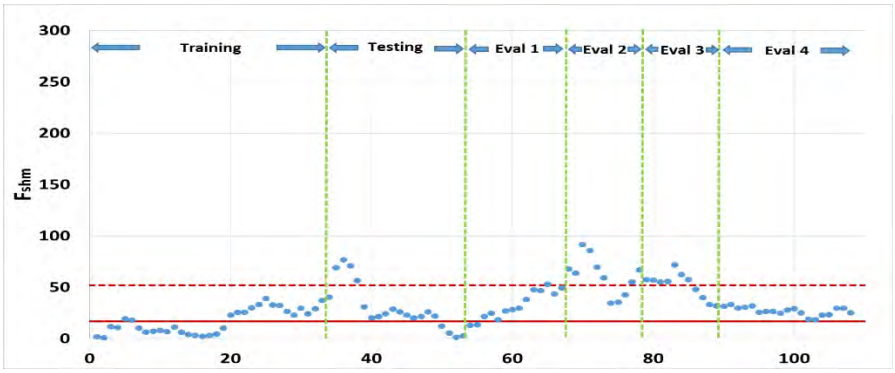

f. C-SG-BF-H vs. C-NG-BF-H

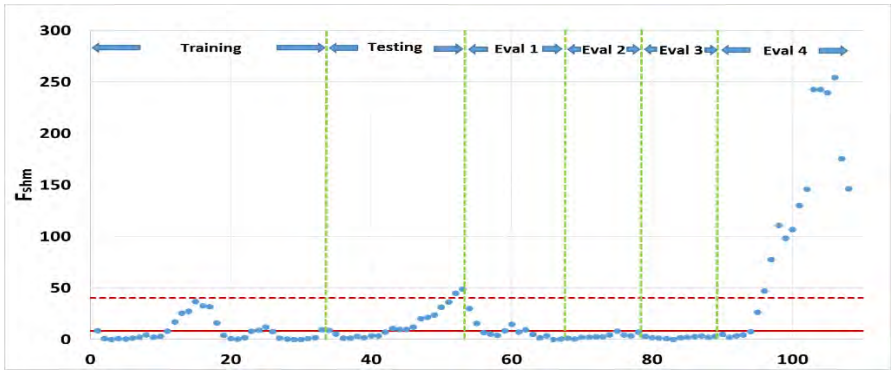

g. C-SG-CB(5)-V vs. C-SG-CB(4)-V

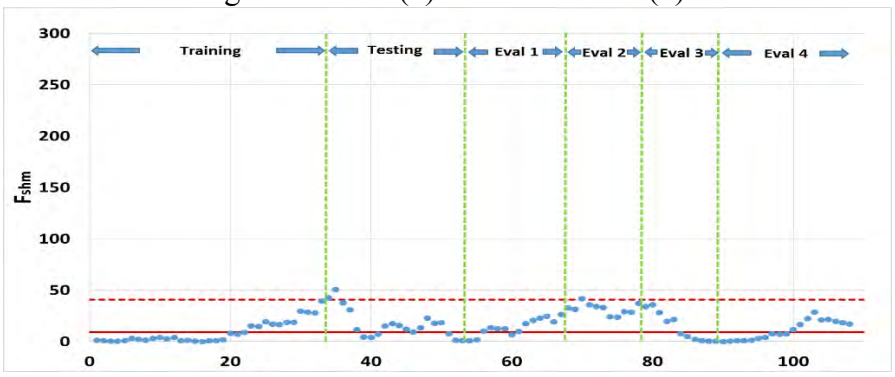

h. C-SG-CB(5)-V vs. C-NG-BF-H

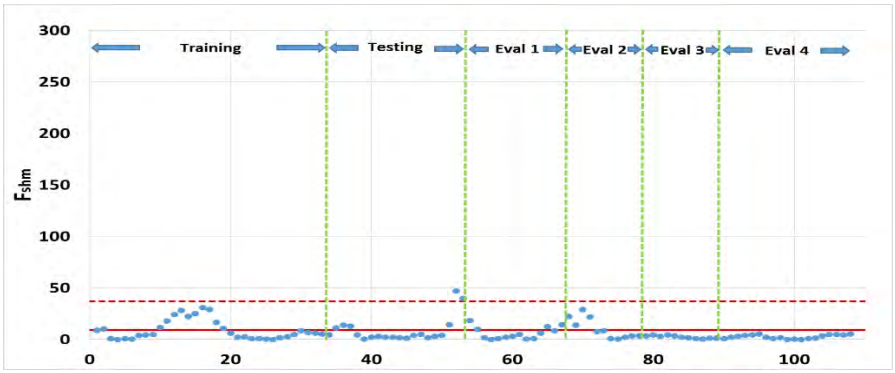

i. C-SG-CB(4)-V vs. C-NG-BF-H

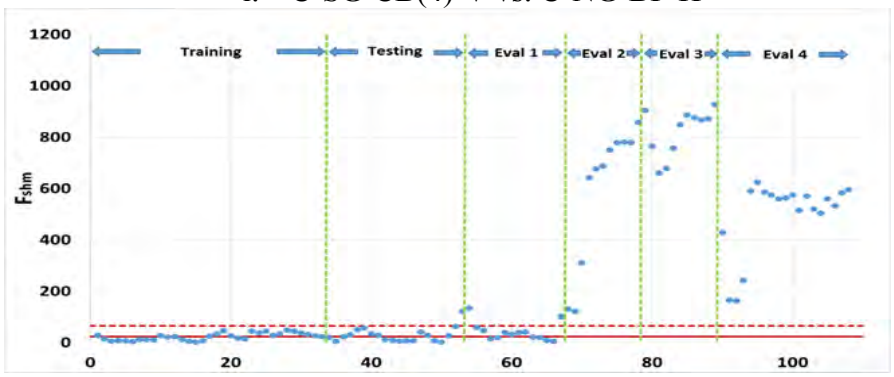

j. B-NG-BF-H vs. Sensor 4 on sacrificial specimen

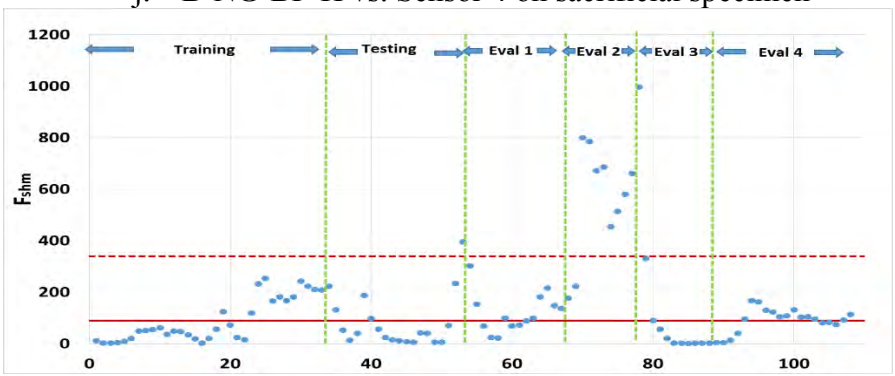

k. B-SG-BF-H vs. Sensor 1 on sacrificial specimen

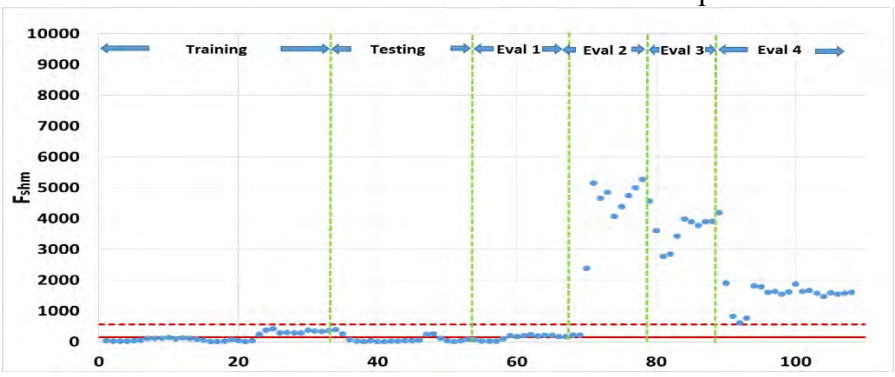

l. B-SG-BF-H vs. Sensor 4 on sacrificial specimen

Figure 4.8. F_{shm} control chart for sacrificial Specimen 2

Tables 4.17 and 4.18 show the number of false indications for sensors on the bridge (non-damaged) and on the sacrificial specimen (near damage), respectively. The F_{shm} method had a higher true-indication rate than the strain range methods, as did the cross prediction method.

Table 4.17. Number of false indications for sensors on bridge (non-damaged) for F_{shm} control chart

Sensor pairs	False indications (Training, Testing, Evaluation 1, 2, 3 and 4)	False indication rate (%)
B-NG-BF-H vs. B-SG-BF-H	113	18.5
B-NG-BF-H vs. C-SG-BF-H	113	18.5
B-NG-BF-H vs. C-SG-CB(5)-V	84	13.7
B-NG-BF-H vs. C-SG-CB(4)-V	76	12.4
B-SG-BF-H vs. C-NG-BF-H	95	15.5
C-SG-BF-H vs. C-NG-BF-H	183	29.9
C-SG-CB(5)-V vs. C-SG-CB(4)-V	109	17.8
C-SG-CB(5)-V vs. C-NG-BF-H	110	18.0
C-SG-CB(4)-V vs. C-NG-BF-H	68	11.1

Table 4.18. Number of false indications for sensors on sacrificial specimen (near damage) for F_{shm} control chart

Sensor pairs near damage	False indications (Training, Testing, Evaluation 1)	False indication rate (%)	True indications (Evaluation 2, 3, and 4)	True indication rate (%)
B-NG-BF-H vs. Sensor 4	33	9.0	155	73.8
B-SG-BF-H vs. Sensor 1	44	12.0	59	28.1
B-SG-BF-H vs. Sensor 4	48	13.1	154	73.3

4.5 Discussion

An objective of the current study was to develop a damage-detection methodology that minimizes the false-detection rate and maximizes the true damage-detection rate. Control chart Rule 1 seems to best characterize the damage-detection ability for all four methodologies. The other rules have excessively high false-indication rates and add little to the true-detection rate.

By and large, the proposed and developed four methodologies detect damage quite well. Figure 4.9 presents a comparison of the false- and true-detection rates. The false-indication rates are

calculated for sensors placed on the bridge where no damage was presumed to have occurred and the true-detection rates are calculated from Sensor 4 near the crack in the sacrificial specimen.

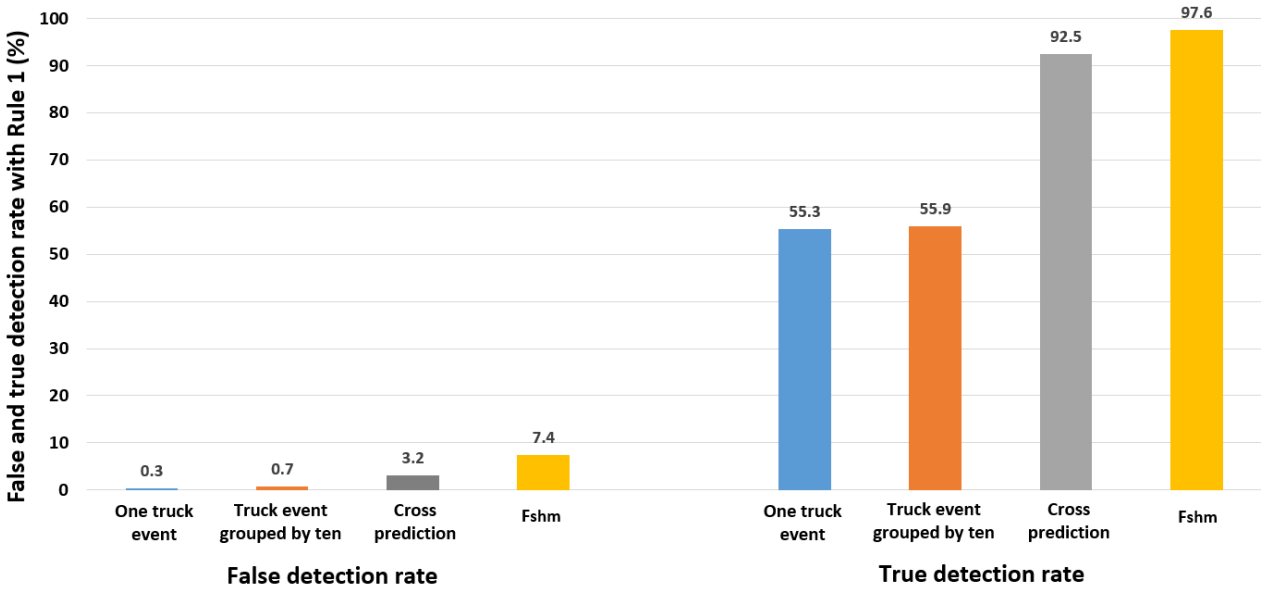

Figure 4.9. False- and true-detection rates with Rule 1

The one-truck methodology, which is the simplest to apply and possibly the most intuitive, has the lowest false-indication rate but also the lowest true-detection rate. The truck events grouped by ten is similar. The two methods (cross prediction and F_{shm}) that pair sensors together with orthogonal regression straight-line fits yield significant improvements in the true-detection rate with, unfortunately, an increase in the false-indication rate.

For all methods, high false-indication rates were found from sensors (C-SG-BF(5)-V and C-SG-BF(4)-V) placed in the cut-back web-gap region of the south girder near the west-most pier. To help the research team understand the cause of the false-detections, the web-gap region was inspected using visual and magnetic particle techniques.

A fatigue crack-like indication was observed as shown in Figure 4.10. As indicated in the photograph, a small crack may be present near the sensor. The depth of the crack is not known.

Given there might be damage near the cut-back web-gap region, further investigation into the false-indication rate was completed by omitting data from the cut-back region. The results are illustrated in Figure 4.11.

Figure 4.10. Photograph of a potential fatigue crack in web cut-back region

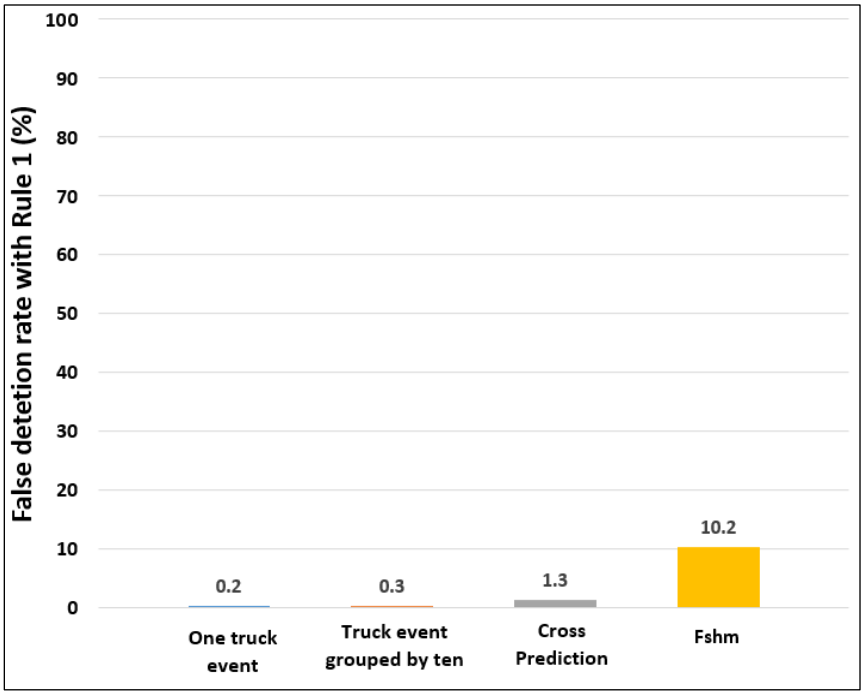

Figure 4.11. False-indication rate without cut-back web-gap region

False-indication rates decreased for the one-truck, truck events grouped by ten, and cross prediction methods. However, the false-detection rate for the F_{shm} method did not decrease because rule violations remained in other non-damaged sensor pairs. Therefore, a challenge in future research would be to achieve the target false-indication rate of 0.3% while maintaining a high true-detection rate.

5. SUMMARY, CONCLUSIONS, AND RECOMMENDATIONS

5.1 Summary

For this project, finalization of hardware and software components for a bridge SHM system were investigated and completed—including a demonstration installation. The goal with this work was to ready a system for widespread implementation.

An SHM monitoring system from previous work on the US 30 Bridge used fiber-optic sensors. In previous work, fiber-optic sensors were also placed on sacrificial specimens connected to the bridge that simulated the structural behavior of the bridge in the cut-back gap area. Varying degrees on damage were introduced into the sacrificial specimen. The data from the fiber-optic system were used in this work to study the performance of four automated damage-detection methodologies.

Although there were many advantages of the fiber-optic sensor system, the hardware system was reconfigured with a traditional sensor system because it was found that a traditional sensor system was more cost-effective and robust. As hoped, the traditional sensor system, installed as a demonstration, operated without failure during the project.

An upgraded external communication system using automated FTP with 4G cellular technology was integrated to transmit the collected data in real-time. BECAS, which is an automated damage-detection process that incorporates sensor data acquisition, strain range data reduction (zeroed and filtered with truck parameter identification), and statistical control charts for four damage-detection methodologies, was developed and implemented.

The four control-chart-based methodologies developed and evaluated in this work are as follows: 1) one-truck event, 2) truck events grouped by ten, 3) cross prediction, and 4) F_{shm}. Control charts utilized by the system developed are divided conceptually into three regions—training, testing, and evaluation—to conveniently allow for study of system operability.

During the training period, strain range data from the undamaged structure were used to establish the required control chart parameters. The testing period followed and was used to check the efficacy of the training period. To monitor the bridge for changes in structural performance, the evaluation period followed immediately after training and testing and was subdivided into regions in this work corresponding to the varying damage levels in the sacrificial specimen.

Six control chart rules were applied to identify changes in structural performance with time. Rule violations, false indications of damage in the undamaged normal structural condition, and true indications of damage in the sacrificial specimen, with respect to each rule, were automatically calculated and then tabulated. In all methodologies, a large number of rule violations were found for Rule 3 and Rule 4. Rules 2, 5, and 6 had fewer false indications but also very few true indications.

The one-truck event method is the most basic form of a control chart reliant upon strain range data without further manipulation and is created using the strain range data for each truck event without further processing. Similar to the one-truck event method, the truck events were grouped with a group size of 10. Both the one-truck event method and the truck grouped by ten method had relatively few false indications. Once damage was introduced into the sacrificial specimen during the evaluation period, both were able to detect damage but with a true-indication rate less than the other methods.

In the cross prediction method, the major enhancement over a previous generation of the approach was in the use of orthogonal regression instead of traditional linear regression. One attractive attribute of the cross prediction method is that it considers each sensor's relationship with other sensors. The cross prediction method had a higher number of false indications than the previous two methods but a significant increase in the number of true indications.

The F_{shm} method is an outgrowth of a method suggested in previous work. As with the cross prediction method, the F_{shm} method uses orthogonal linear regression for paired strain range data. Unlike the first three methods, one F_{shm} control chart represents each pair. This results in a very large number of control charts. The false-indication rate and true-indication rate are similar to the cross prediction method.

5.2 Conclusions

Based on the completed work for this project, the following conclusions are made:

- BECAS automates all of the components of a full SHM system successfully

- As with all SHM methods, separating true structural performance data from monitoring system noise is a major challenge and, with this work, progress has been made in this direction by:
  - Implementation of orthogonal linear regression
  - Evolution of the F_{shm} method to improve true positive damage indications

- The target false-alarm rate of 0.3% was achieved with the one-truck event method; however, the highest true-indication rate was achieved with the F_{shm} method

- Possible damage in the cut-back region of one girder was detected by multiple damage-detection methods

5.3 Recommendations for Future Work

For future work, additional work is required to obtain a damage-detection methodology that achieves the target false-indication rate (i.e., 0.3%) while at the same time ensuring a high true-indication rate.

Preliminary work related to this improvement leads the research team to believe that this work should focus on reducing the effect of strain gauge reading uncertainty. This reduction in strain gauge uncertainty fits well in the previously-completed work aimed at decreasing uncertainty associated with selecting live load events meeting specific criteria.

REFERENCES

Caragea, Petruta C. *The F-Test as a Comparison of Full and Reduced Models*. Iowa State University. Ames, Iowa. Fall 2007.

Carroll, R. J., and D., Ruppert. "The Use and Misuse of Orthogonal Regression Estimation in Linear Errors-in-Variables Models." *The American Statistician*, 1996.

Doornink, J. D. Monitoring the Structural Condition of Fracture-Critical Bridges Using Fiber Optic Technology. PhD dissertation. Iowa State University, Ames, Iowa. 2006.

Fuller, W. A. *Measurement Error Models*. New York: John Wiley & Sons, Inc., 1987.

Lu, P., Phares, B. M, Greimann L., Wipf, T. J. "Bridge structural health-monitoring system using statistical control chart analysis," *Journal of the Transportation Research Board*. No. 2172, pp. 123-131, 2010.

Lu, P., A statistical based damage detection approach for highway bridge structural health monitoring. PhD dissertation. Iowa State University. Ames, Iowa. 2008.

Mendenhall, William, and Terry Sincich. *A Second Course in Statistics: Regression Analysis*. Seventh Edition. Boston, Massachusetts: Prentice Hall/Pearson Education, Inc. 2012.

Miller, I., and J. E. Freund. *Probability and Statistics for Engineers*. Second Edition. Englewood Cliffs, New Jersey: Prentice-Hall, Inc.1977.

Montogomery, D. C. *Introduction to Statistical Quality Control*. Third Edition. New York: John Wiley & Sons, Inc. 1996.

Phares, B., Wipf, T., Lu, P., Greimann, L., and Pohlkamp, M. *An Experimental Validation of a Statistical-Based Damage Detection Approach*. Bridge Engineering Center, Iowa State University, Ames, Iowa. 2011.

Vis, James M. *Evaluation of a Structural Health Monitoring System for Steel Girder Bridges*. MS Creative Component Report. Iowa State University, Ames, Iowa. 2007.

Wipf, T. J., Phares, B. M., and Doornink, J. D. *Monitoring the Structural Condition of Fracture-Critical Bridges Using Fiber Optic Technology*. Bridge Engineering Center, Iowa State University, Ames, Iowa. 2007.

APPENDIX A. SPECIFICATIONS FOR THE FIBER-OPTIC SENSORS IN THE US 30 SHM SYSTEM

Channel	FOS Name	Grating length (mm)	Central Wavelength (nm)	Sensor ID
Channel 1	B-NG-BF-H	10	1517.5	1
	B-NS-BF-H	10	1522.5	2
	B-SS-BF-H	10	1527.5	3
	B-SG-BF-H	10	1532.5	4
	C-SG-BF-H	10	1537.5	5
	C-FB(SS)-BF-H	10	1542.5	6
	C-SS-WB-V	10	1547.5	7
	C-SG-CB(5)-V	5	1552.5	8
	C-SG-CB(4)-V	5	1557.5	9
	C-SG-CB(3)-V	5	1562.5	10
	C-SG-CB(2)-V	5	1562.5	11
	C-SG-CB(1)-V	5	1567.5	12
	A-NS-WB-V	10	1577.5	13
	A-SS-WB-V	10	1582.5	14
Channel 2	D-SG-BF-H	10	1517.5	15
	D-SS-BF-H	10	1522.5	16
	D-NS-BF-H	10	1527.5	17
	D-NG-BF-H	10	1532.5	18
	C-NG-BF-H	10	1537.5	19
	C-FB(NS)-BF-H	10	1542.5	20
	C-NS-WB-V	10	1547.5	21
	C-NG-CB(5)-V	5	1552.5	22
	C-NG-CB(4)-V	5	1557.5	23
	C-NG-CB(3)-V	5	1562.5	24
	C-NG-CB(2)-V	5	1567.5	25
	C-NG-CB(1)-V	5	1572.5	26
Channel 3	E-NG-BF-H	10	1517.5	27
	E-NG-CB(5)-V	5	1522.5	28
	E-NG-CB(1)-V	5	1527.5	29
	E-NS-WB-V	10	1532.5	30
	E-FB(NS)-BF-H	10	1537.5	31
	E-FB(SS)-BF-H	10	1542.5	32
	E-SS-WB-V	10	1547.5	33
	E-SG-CB(5)	5	1552.5	34
	E-SG-CB(1)-V	5	1557.5	35
	E-SG-BF-H	10	1562.5	36
	F-SG-BF-H	10	1567.5	37
	F-SS-BF-H	10	1572.5	38
	F-NS-BF-H	10	1577.5	39
	F-NG-BF-H	10	1582.5	40
Channel 4	Sensor 1	5	1562	41
	Sensor 2	5	1567	42
	Sensor 3	5	1572	43
	Sensor 4	5	1577	44

APPENDIX B. SETTING UP FTP DATA SYNCHRONIZATION PROCESS USING BESTSYNC 2013

The File Transfer Protocol (FTP) data synchronization process utilized the software BestSync 2013 and the set up is described in this appendix. The first step is to set up an office FTP server with login account information including username, password, and IP address. Next, start BestSync and select Edit then Add Task as shown in Figure B.1.

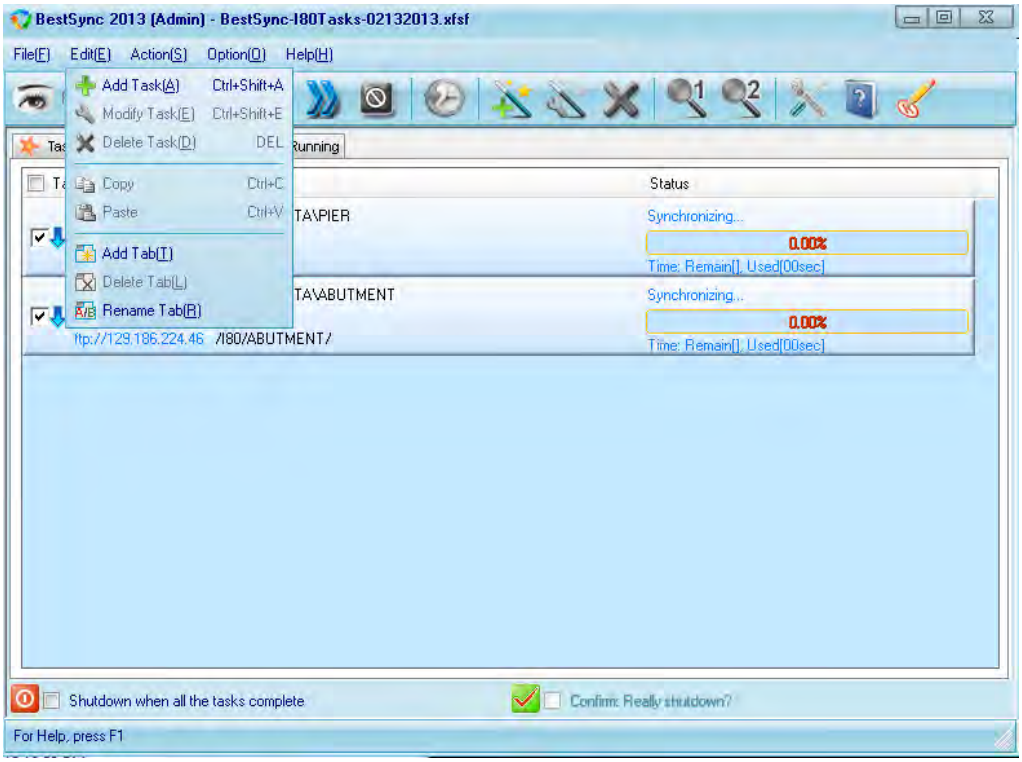

Figure B.1. BestSync startup

Start by selecting the Folder1 magnifying glass and then select the proper Synchroniation Direction. In most cases, select the Folder1 to Folder2 only as shown. This transfers files from the remote desktop PC to the Office FTP Server only as shown in Figure B.2.

Figure B.2. File transfer

Next, select the File Folder option and choose the location where the sensor data are being stored on the desktop computer at the remote site and finish by clicking OK as shown in Figure B.3.

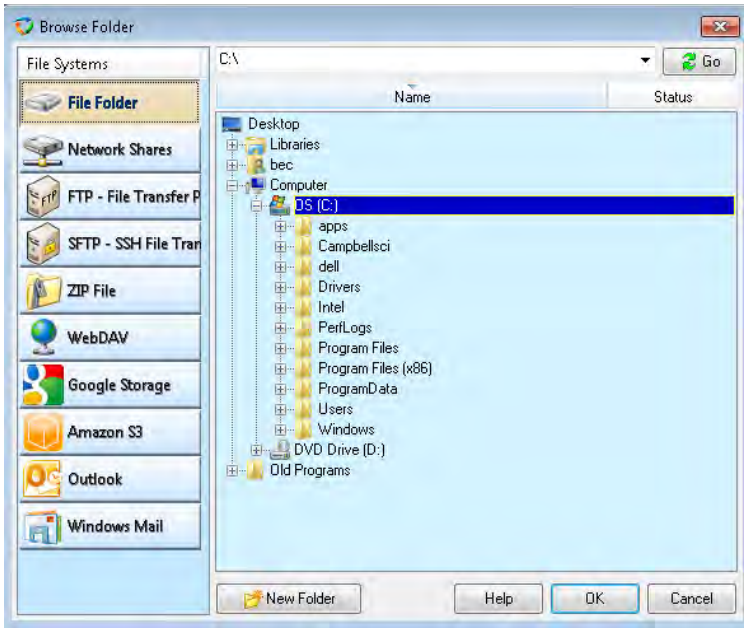

Figure B.3. Data storage location

Subsequently, select the Folder2 magnifying glass as shown in Figure B.4.

Figure B.4. Folder destinations

Choose the FTP – File Transfer Protocol option and enter the FTP Server information as shown in Figure B.5 and click OK.

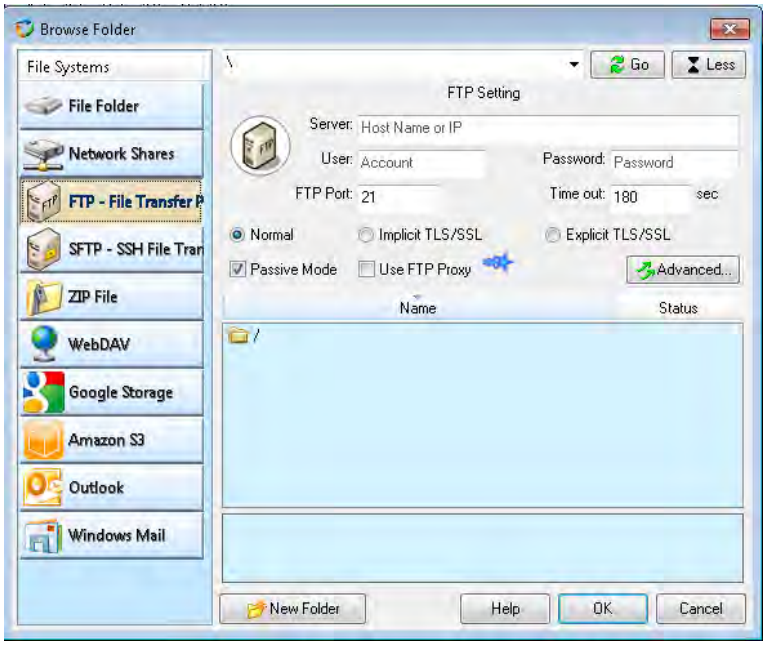

Figure B.5. FTP server info

Afterward, give the task a name and click Next as shown in Figure B.6.

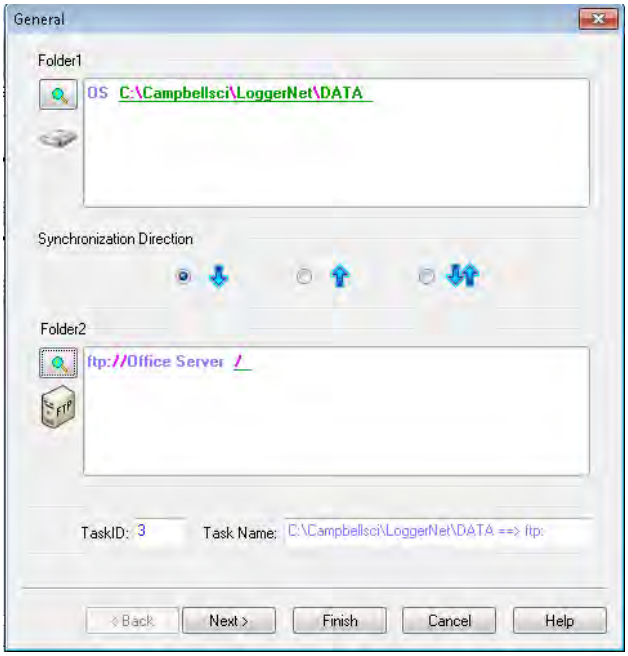

Figure B.6. Task name

A backup option may be specified. However, in most cases this option will not be used so uncheck the Enable box as shown in Figure B.7.

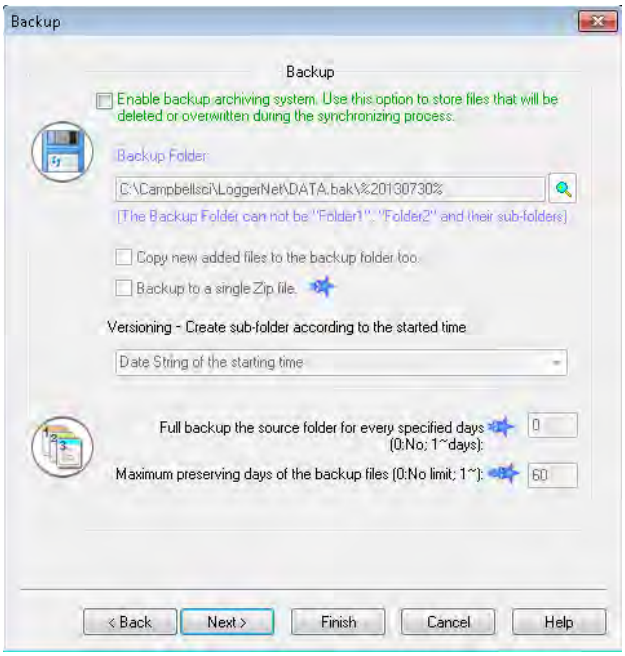

Figure B.7. Backup option

Next, add any specific excludes or includes. Note that this part is typically left blank. as shown in Figure B.8, and proceed by clicking Next.

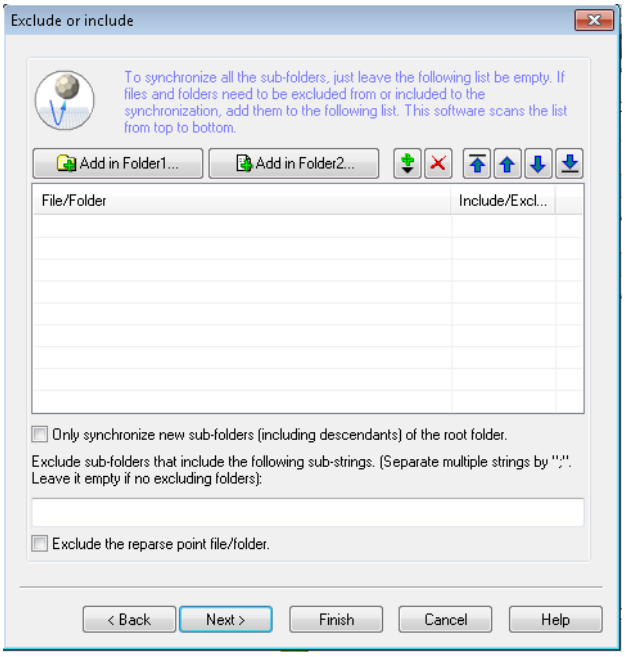

Figure B.8. Exclude or include

This next process involves entering a file filter if different sets of logger files are located in the data folder. First, uncheck the Include subfolders checkbox and check the Ignore the file if it is changed and less than this…. Then, enter a number of seconds to keep the sync process from trying to transfer files before they have been written completely from the logger. Note that this may take some adjustment to get the proper time limits given that it depends on how fast the logger is able to write files to the remote PC hard drive. Finally, check the Only scan the source folder to detect if files are changed… checkbox and then click Next. As shown in Figure B.9, this filter will only get .dat files that begin with CR9000X and the * is a wildcard option.

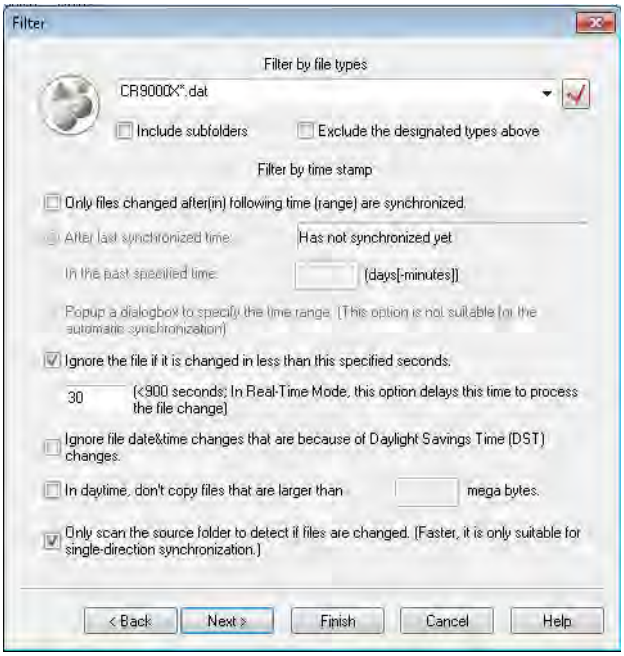

Figure B.9. Filter files

In the subsequent process, duplicate the checkbox settings shown in Figure B.10. The maximum thread number can and should be adjusted to accommodate transfer rates of the internet service being used. It is recommended to use 1 to 3 files maximum on 3G service and 1 to 8 files maximum for broadband or 4G service. Finish by clicking Next and click next for the subsequent window shown in Figure B.11.

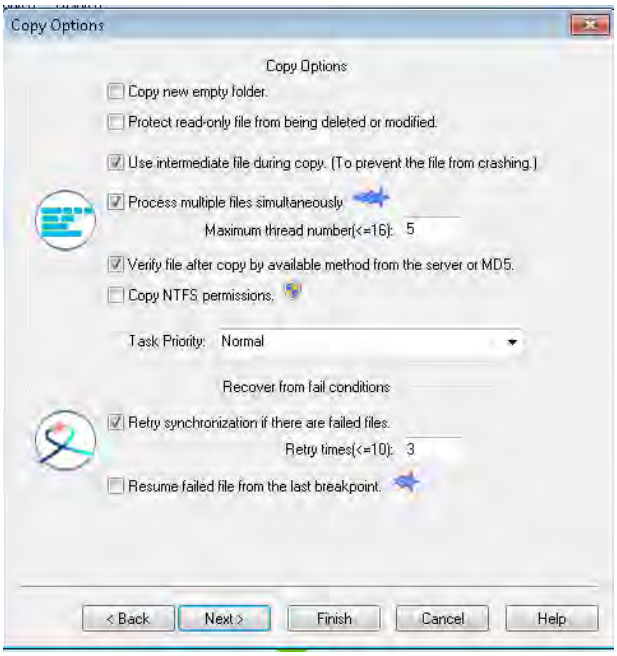

Figure B.10. Copy options

Figure B.11. Volume shadow copy

The subsequent windows should be as shown in Figure B.12, B.13, and B.14.

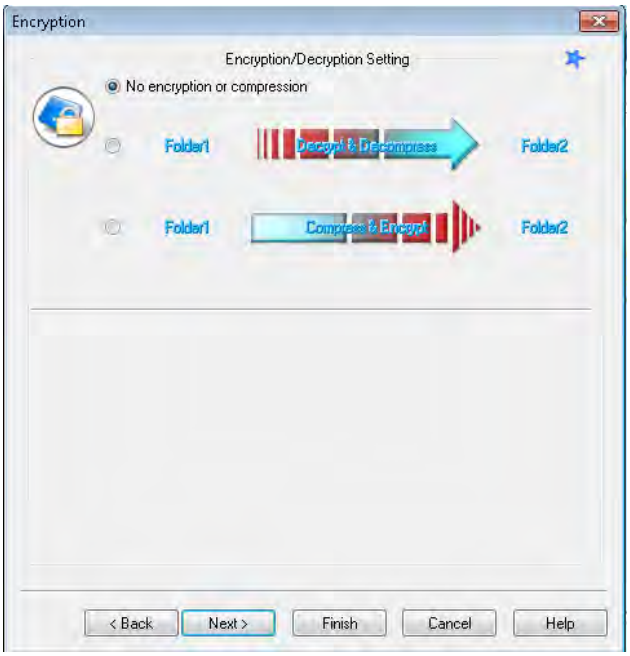

Figure B.12. Encryption

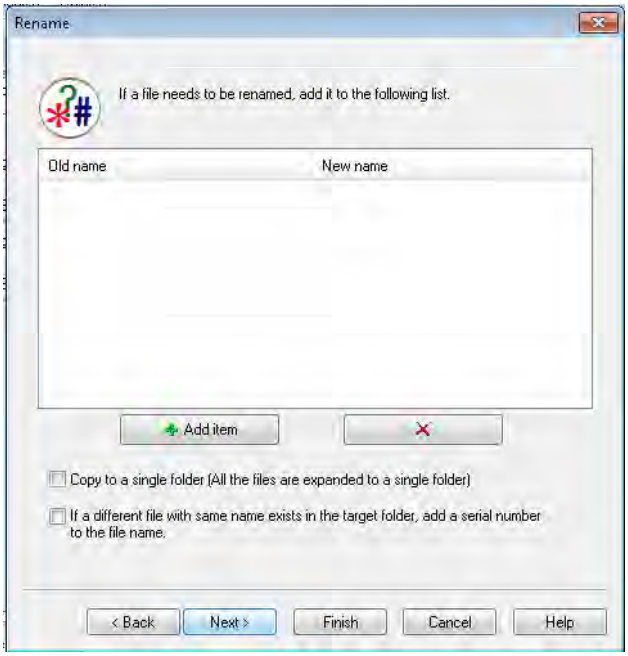

Figure B.13. Naming

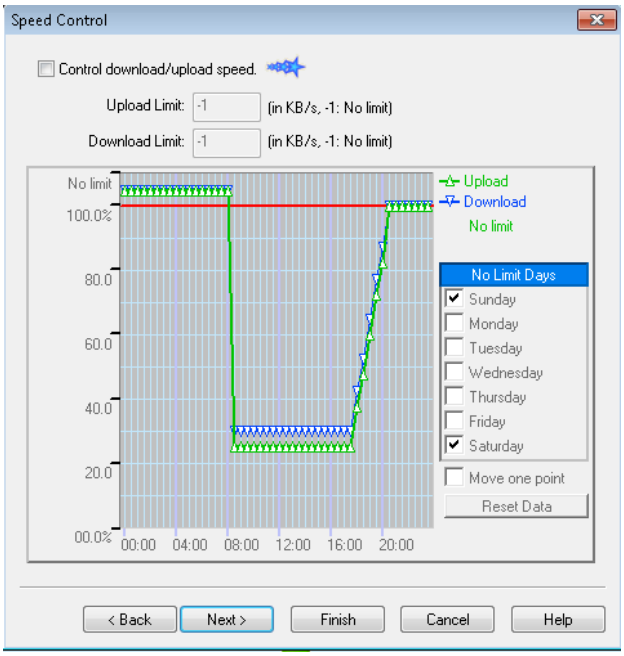

Figure B.14. Speed control

Depending on the data being retrieved, there are a couple of options for the timing after checking Service Sync... The first option is to run Real-Time Sync by checking the appropriate box as shown in Figure B.15. The second option is to select a rate that is appropriate to the logger data collection rate, such as every minute as shown in Figure B.16.

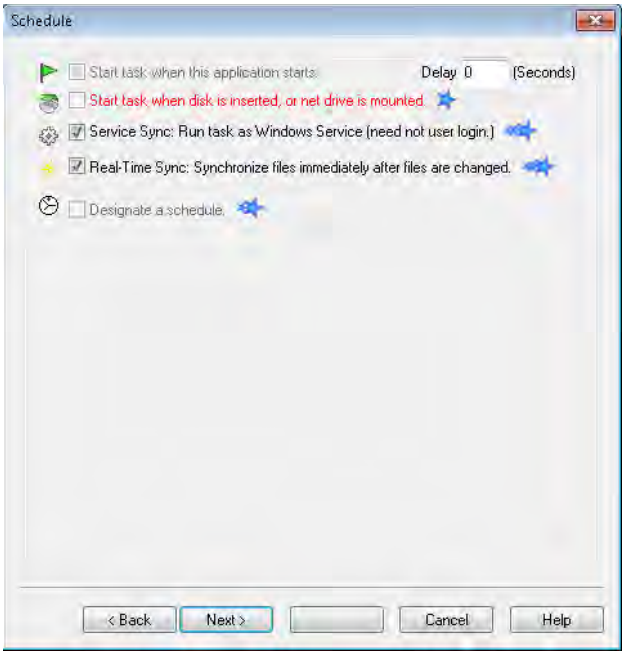

Figure B.15. Schedule real-time sync option

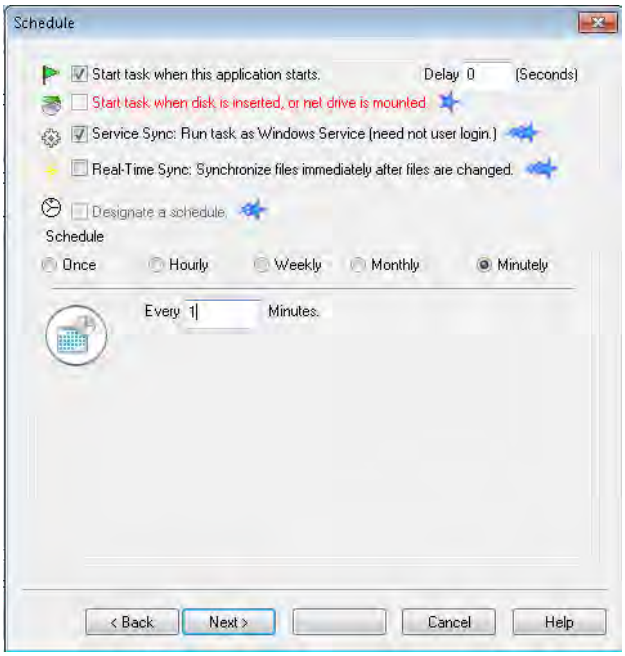

Figure B.16. Schedule time option

Next, uncheck Record the log data for the log view window as shown in Figure B.17 and click Next.

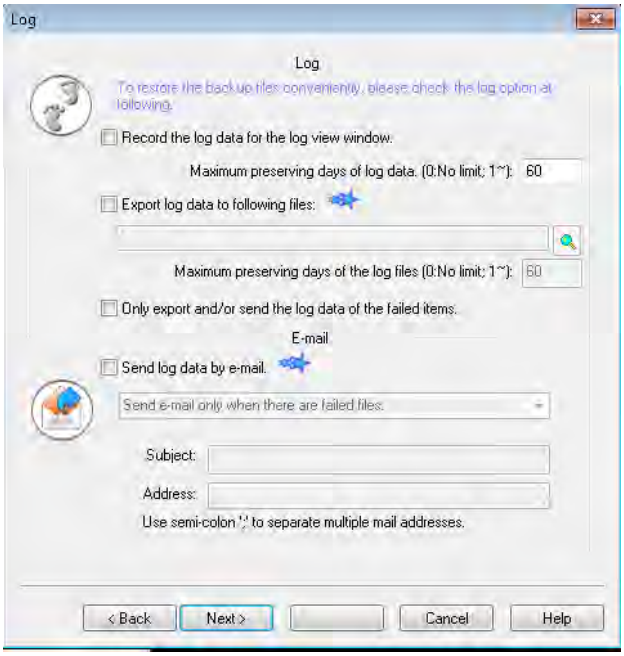

Figure B.17. Log

Click Finish as shown in Figure B.18.

Figure B.18. Application

Save the process by clicking File, Save As as shown in Figure B.19 and Save a copy of the backup process in case it needs to be reloaded; otherwise, the process will need to be recreated from scratch.

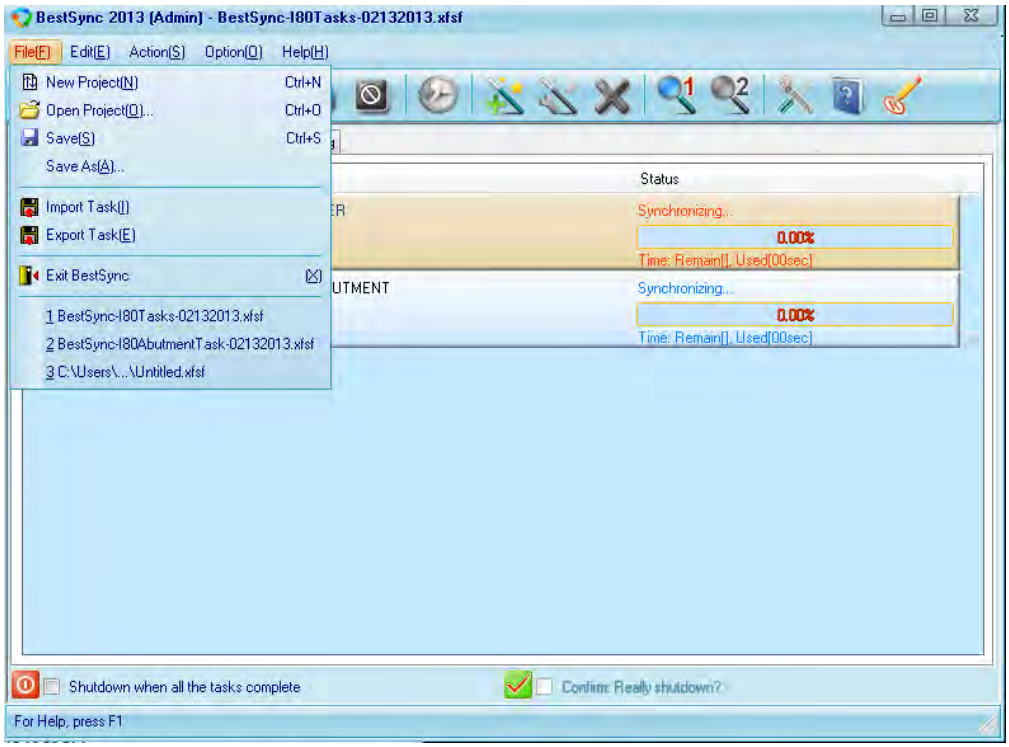

Figure B.19. Save